Five millennia of human-environment interactions reconstructed from pedosedimentary archives of the Lac du Puy wetland (Corent, Fr.)

Alfredo Mayoral, Jean-François Berger, Jean-Luc Peiry, Paul Ledger, Yannick Miras

FIVE MILLENNIA OF HUMAN-ENVIRONMENT INTERACTIONS RECONSTRUCTED FROM PEDOSEDIMENTARY ARCHIVES OF THE LAC DU PUY WETLAND (CORENT, FR.)

MAYORAL, ALFREDO (1); BERGER, JEAN-FRANÇOIS (2); PEIRY, JEAN-LUC (3); LEDGER, PAUL (4, 5); MIRAS, YANNICK (6)*

1. Université Clermont Auvergne, CNRS, GEOLAB, F-63000 Clermont-Ferrand, France & Catalan Institute of Classical Archaeology, Pl. Rovellat s/n, 43003 Tarragona, Spain.

2. CNRS, UMR 5600, EVS-IRG & Université Lyon 2, Lyon, France

3. Université Clermont Auvergne, F-63000 Clermont-Ferrand & CNRS, EDYTEM, F-73000 Chambéry, France

4. Department of Archaeology, Memorial University of Newfoundland, St. John's, Newfoundland, Canada

5. Department of Geography, Memorial University of Newfoundland, St. John's, Newfoundland, Canada

6. CNRS, UMR7194, Histoire Naturelle de l'Homme Préhistorique, Département de Préhistoire, Muséum National d'Histoire Naturelle, Institut de Paléontologie Humaine, Paris, France & Université Clermont Auvergne, CNRS, GEOLAB, F-63000 Clermont-Ferrand, France

*Corresponding author: alfredo.mayoral@uca.fr

Abstract

This paper presents a multi-proxy geoarchaeological analysis of the complex pedo-sedimentary archives of a small pond situated within the protohistoric site of Corent, in central France. A robust chrono-stratigraphic framework was developed integrating all chronological data from previous studies. Micromorphological, geochemical and sedimentological analyses were performed on a

radiocarbon-dated core. Results are discussed alongside palynological data from previous work on the same core, in order to reconstruct human-environmental interactions on the Corent volcanic plateau since the Neolithic. After intense soil erosion recorded during the Early and Middle Neolithic, the Late Neolithic is characterized by vegetation recovery and soil stability in the basin contemporaneous with site abandonment, perhaps due to pronounced soil degradation in the plateau. During the Early Bronze Age, agropastoral land use contributed to major environmental changes in the pond's basin, including soil profile sealing and gleyfication. Environmental impact patterns detected in the pedo-sedimentary record indicate settlement intensification during the Middle Bronze Age. After the substantial impacts of an intense anthropogenic disturbance in the Early Iron Age, the Lac du Puy becomes a vertic depression recurrently flooded while a late Iron Age Gallic *oppidum* develops on the plateau, and is finally backfilled at the end of the Iron Age. The detailed multi-proxy picture from this intra-urban wetland helps nuance our understanding of the environmental impacts of prehistoric societies in Western Europe. Indeed, our results highlight the importance of keeping a long term perspective when dealing with past human-environment interactions.

Keywords: Human-environment interactions; Pedo-sedimentary archives; Geoarchaeology; Soil Micromorphology; Palaeosoils; Limagne; Holocene

1-Introduction

Long-term human-environment interactions and the gradual 'anthropogenization' of natural systems are topics that have been widely investigated and discussed in geoarchaeological, palaeoenvironmental and environmental archaeological studies, from western Europe in recent decades (e.g. van der Leeuw et al., 2005; Dearing, 2006; Berger et al., 2007; Butzer, 2011; Notebaert

& Berger, 2014; Carozza et al., 2015; Arnaud et al., 2016; Cremaschi et al., 2016; Lespez et al., 2016). More recently renewed research momentum has been stimulated by the emergence of the hotly debated 'anthropocene' paradigm (Crutzen & Stoermer, 2000; Foley et al., 2013; Cremaschi, 2014; Butzer, 2015; Lewis & Maslin, 2015; Verstraeten, 2015; Ruddiman et al., 2015; Ruddiman, 2017; Bauer & Ellis, 2018).

Off-site palaeoenvironmental and geoarchaeological research (e.g. in lakes, peatlands, floodplains etc.) continue to provide valuable records of human impacts in environmental dynamics (e.g. Miras et al., 2004; Brown et al., 2013; Arnaud et al., 2016; Berger et al., 2016; Peña-Monné, 2018; Dubois et al., 2018). In addition, progress in site-based geoarchaeological approaches is producing large amounts of detailed archaeometric data related to human-environment interactions (Butzer, 2008). Improvements in our understanding of Holocene palaeoclimatic change are allowing the development of detailed analyses of the interaction between climate and society (Magny et al., 2009; Armit et al., 2014; Lespez et al., 2016; Roberts et al., 2019). Together, these new data contribute to feed scientific discussion and to improve our understanding of the progressive anthropogenic forcing of natural systems through the Middle to Late Holocene.

Despite these achievements some "grey zones" remain in human-environment interaction studies, often neglected by palaeoenvironmental and geoarchaeological works. This is typically the case for human-environment interface halfway between site-based and off-site contexts, as researchers regularly focus on areas suitable for the formation and preservation of "optimal" sedimentary records, that are able to provide unambiguous interpretations. Intermediate, or "site-proximal" contexts are often neglected due to their sometimes incomplete sedimentary records, signal complexity or poor taphonomic conditions (Ledger et al., 2015, 2017).

These "site-proximal" contexts are nevertheless crucial for developing an integrated understanding of the complex nature of long term human-environment interactions. They provide unique and sensitive records of processes characteristic of transitional zones, displaying a mixture of natural and

cultural features. This makes them useful for characterizing human-environment interaction, such as locally increased impacts related to proto-urban emergence (Kaniewski et al., 2013; Danielisova and Hajnalova, 2014; Ledger et al., 2015; Styring et al., 2017). Formation processes of pedosedimentary sequences on the periphery of archaeological sites, often marked by hiatuses and cumulated dynamics, are valuable yet complex palimpsests that present a real geoarchaeological challenge, and are fertile ground for multi-proxy approaches. Wetlands under human influence are similar case and they have been widely studied from a palaeoenvironmental and geoarchaeological perspective in rural areas (e.g. Martín-Puertas et al., 2009; Macaire et al., 2010; Bernigaud et al., 2014; Hausmann et al., 2018; Haas et al., 2019), but site-proximal or intra-site wetlands are rare and consequently less frequently studied.

Geographical Settings and Archaeological Background

The Lac du Puy is typical of these rare contexts. The small wetland is situated within the extension of the large protohistoric archaeological site of Corent, located on a volcanic plateau dating from the Pliocene (Greffier et al., 1980; Nehlig et al., 2003; Mayoral et al., 2018). The plateau is located in a commanding position, controlling the north-south axis of the valley of the River Allier, 20 km south of Clermont-Ferrand (French Massif Central, see Fig. 1). The southern part of the plateau is a scoria cone with moderate slopes, while the Lac du Puy basin is situated in the northern area of the plateau, a basaltic lava flow with gentle topography. It is a closed circular depression (c. 2 Ha) interpreted as a pseudo-sinkhole (Mayoral et al., 2018), nowadays occupied by a dry (but seasonally wet) agricultural field with a small drained pond (20x20m) fed by runoff and subsurface flow. Aerial photography and historical maps suggest that before drainage operations in the early XIXth century (Ledger et al., 2015), the open water area in the depression was probably more extensive (c. 100x80m) and could perhaps have been a valuable water source.

Extensive archaeological excavation at Corent since the 2000's has shown human occupations spanning from Middle Neolithic to Roman period. The Middle Neolithic, dated c. 4200-3700 BCE

(Before Common Era), is characterized by a large fortified settlement and ditched structures (Poux et al., 2018). Later, a collective burial was installed in the summit of the plateau (Daugas, 1972), maybe in the Late Neolithic (c. 3000-2400 BCE). The Bronze Age is characterized by several occupations. The most studied is a Late Bronze Age III (950-800 BCE) agglomerated settlement with proto urban features, which given its hilltop position and size is unique in France (Milcent et al., 2014a; Ledger et al., 2015). Centuries later in the Early Iron Age (Hallstatt D1, 625-510 BCE) a proto-urban settlement developed as is seen elsewhere in Western Europe (Milcent et al., 2014b; Fernández-Götz, 2018). The most celebrated phase of the site is undoubtedly the Late Iron Age *oppidum* (La Tène D1-2 140-30 BCE). This was an immense, monumental and wealthy urban centre including public, artisanal, religious and commercial buildings, which was probably the capital of the *Arverni* (Poux, 2012; Milcent et al., 2014b; Poux et al., 2018). After the Roman conquest, the site became a well-developed secondary agglomeration (30 BCE-300 CE , Poux et al., 2018).

This trajectory of successive occupations makes Corent an important site in European protohistory with rich potential for analyzing long-term socio-environmental interactions, and human impacts during proto-urban and urban episodes of the 1st millennium BCE. Surprisingly, the palaeoenvironmental and geoarchaeological potential of the wetland has long time been neglected, aside from a restricted archaeological survey in the early 1990s (Guichard, 1991).

Summary of recent research and Objectives

In the framework of the AYPONA palaeoenvironmental program, begun in 2013, palynological research (Ledger et al., 2015) and geoarchaeological survey (Mayoral and Depreux, 2017; Mayoral et al., 2018) were undertaken within this wetland. The objectives were to investigate long-term human-environment interaction, impacts of human settlements since the Neolithic, and localized impacts during the proto-urbanization episodes of the I[st] millennium BCE.

Palynological investigations analyzed (pollen and NPPs) half of a sedimentary core extracted in the Lac du Puy basin and developed an age-depth model based on radiocarbon dating (see Ledger et al., 2015). The results indicated more or less continuous human impact from the Neolithic until the Roman era. The Neolithic to Middle Bronze Age was characterized by a classical pattern of woodland clearance and landscape opening, coupled with the gradual intensification of agriculture, and development of pastoral activity. From the end of the Late Bronze Age, there is evidence of increased biodiversity, plants indicative of ruderal environments and limited evidence of agriculture. These patterns, together with other key features such as occurrences of non-native plant taxa, were interpreted as those of emerging proto-urban areas in the Late Bronze Age and the Late Iron Age (Ledger et al., 2015). Further geoarchaeological research involved trench-based survey, developed in 2015 (Mayoral et al., 2018). The infilling of the basin, divided in 12 Stratigraphic Units (SU), is in general clayey and ranges from 30 cm to 2m in deeper central sectors of the basin, with very variable depth and often sharp lateral changes of pedo-sedimentary facies (Fig. 1F).

Geomorphology and stratigraphy from logs and cross-sections, geophysics, radiocarbon dating and archaeological findings were used to build a first chrono-stratigraphic framework at the scale of the basin, and ultimately to outline the main phases of its complex pedo-sedimentary and hydrological evolution (Fig. 1F&G, adapted from Mayoral et al., 2018). The first phase of the infilling of the basin starts somewhere at the end of the Early, or in the beginning of the Middle Neolithic (before 4500 cal. BCE). Sparse pools in the irregular basaltic bedrock revealed by geophysics (Fig. 1D) received strong runoff bringing scoria and clays (SU6A/B), whereas a weathering profile had started to develop over basalts in higher areas (WB). By the Middle Neolithic (circa or after 4500 cal. BCE), an oscillating water table and detrital sedimentary inputs smoothed the irregular topography of the basin (SU5A-B-C, Fig. 1F&G). Fragmentary archaeological remains are indicative of human activity in the area, maybe related to contemporaneous occupations of the plateau. Following this phase, a very low deposition rate, or even a hiatus between SU5 and SU4, makes interpretation of the depositional environment difficult (Mayoral et al., 2018). A new sedimentary phase, beginning in the

148 Early to Middle Bronze Age (1900-1600 cal. BCE), was characterized by low-energy environment and
149 high watertable level (clayey gleysol, SU4-4a1-4b; see Fig. 1F&G). At the top of this unit, is an
150 archaeological soil containing *in-situ* structures dating to the Late Bronze Age 3 (950-800 BCE). This
151 unit is almost certainly associated by the contemporaneous LBA3 occupation of the plateau and
152 indicates human activity in the basin at this time. Following this period, and until the fifth century BC,
153 sedimentation was interrupted coinciding with a soil stability phase in the plateau. However shortly
154 after (600-425 BCE), the digging of c. one thousand storage pits, probably associated by the
155 neighboring Hallstatt D settlement, massively disturbed pedo-sedimentary and hydrological
156 dynamics of the basin (Fig. 1F&G). After abandonment of these pits, the disturbance period was
157 followed by deposition of SU3, characterized by ephemeral flooding, detrital inputs and vertisol-type
158 dynamics (seasonal shrink-swell processes). In the late Iron Age (La Tène D, 100-40 BCE) at least two
159 phases of soil leveling and backfilling affected southern parts of the basin (SUA1-A2), followed by a
160 generalized leveling and backfill of the Lac du Puy (50/40-30 BCE, SU2). These backfill layers, always
161 associated with archaeological structures, are characterized by heterogeneous grain-size, very
162 frequent basaltic and amphorae inclusions, homogeneous thickness in all their extent, and abnormal
163 or erosive stratigraphic contacts (Fig. 1F). Indeed, they partly truncate positive reliefs on SUs 3 and 4
164 (Fig. 1F&G). These earthworks were caused by the gradual extension of the Gallic oppidum and were
165 certainly accompanied by drainage (Mayoral et al., 2018). After Antiquity, sedimentation slowly
166 covered antique backfill and a topsoil with incipient vertic features developed (SU1) as wet
167 conditions gradually returned, until the depression was drained in recent centuries.

168 In summary, previous palynological and geoarchaeological research provided the first chrono-
169 stratigraphic framework for the basin, and revealed the human influences likely driving its
170 development since the Neolithic. However, the precise relationship between changing pedo-
171 sedimentary processes and human activity remains unclear. For instance, were Neolithic detrital
172 inputs connected with woodland clearance detected by palynology and with occupation phases of
173 the plateau? Were the gleyic conditions at the onset of the Bronze Age related to human activity?

How did the vertisolization processes following the abandonment of storage pits in the Iron Age develop? Similarly, the *hiatus/*low-deposition phases were hindering comprehensive understanding of the sequence, and required more detailed examination.

This work aims to resolve these questions by applying an integrative and high-resolution geoarchaeological approach to the rich but complex pedo-sedimentary archives of the Lac du Puy. A multi-proxy geoarchaeological analysis was performed on a sedimentary core from the deepest area of the basin (Fig 1D), well-representative of the pedo-sedimentary sequence of the lower areas of the Lac du Puy (Fig. 1E&G). New micromorphological analyses, completed with high-resolution sedimentological and geochemical data, were integrated with previous palynological and archaeological information. Results were interpreted within a refined chrono-stratigraphic framework based on a compilation and integration of available radiocarbon, archaeological and stratigraphic evidence.

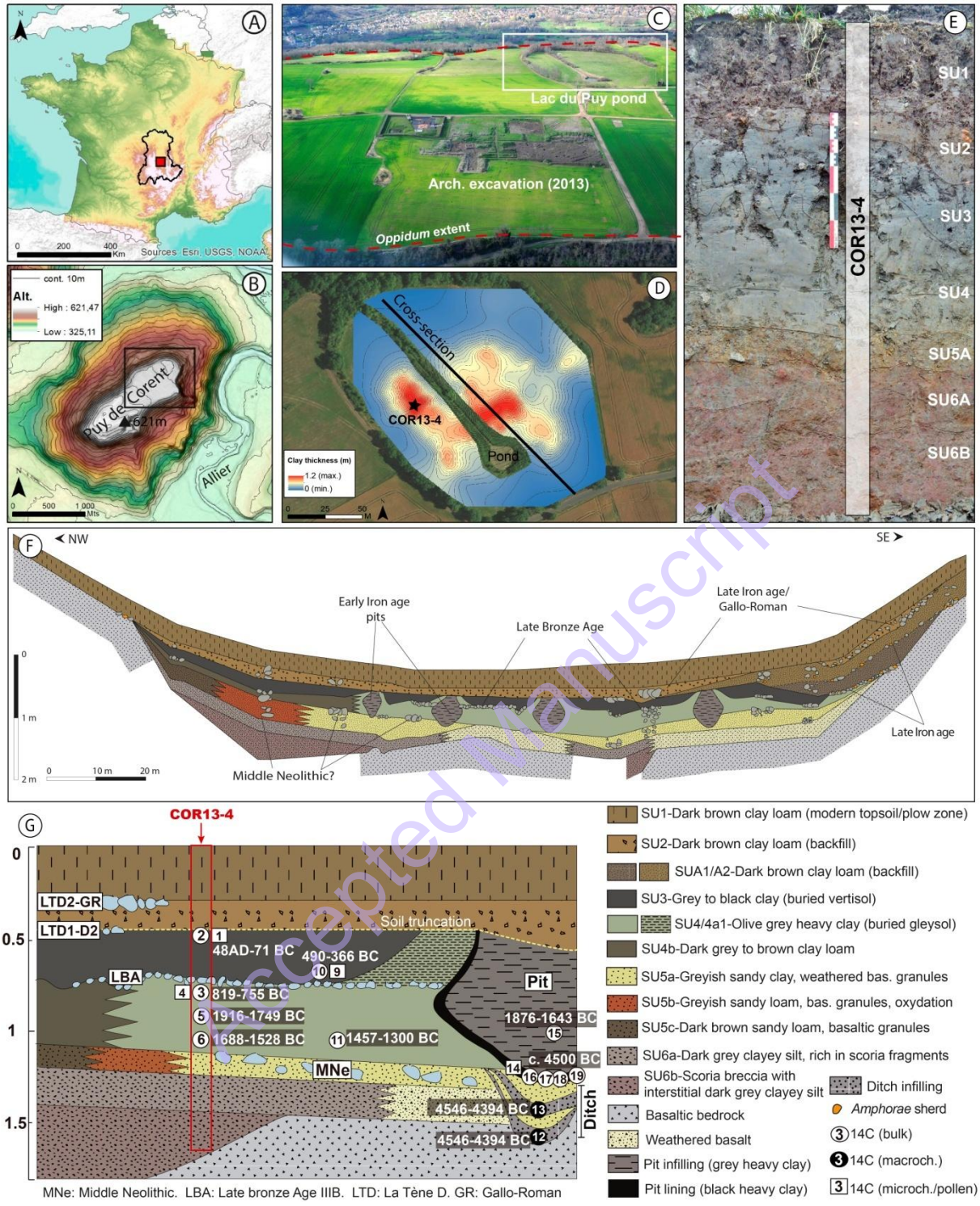

MNe: Middle Neolithic. LBA: Late bronze Age IIIB. LTD: La Tène D. GR: Gallo-Roman

Figure 1. A) Location of study site in central France. Black line delineates Auvergne region. B) Location (black frame) of archaeological site and the Lac du Puy pond in lower part of the plateau of Corent. C) Aerial view of the Lac du Puy and the archaeological excavation (2013), with the known *oppidum* extent (red dashed line). Image credits: B. Dousteyssier. D) Depth model of the clayey infilling of the Lac du Puy basin (Mayoral and Depreux, 2017) with location of core COR13-4 and cross-section shown in F. Clayey infilling is thicker in red areas. No data are available on the today water body and its drainage (central part of the basin). E) Profile section corresponding exactly to core COR13-4. F) Stratigraphic cross-section of the Lac du Puy, modified from Mayoral et al. 2018. G) Chrono-stratigraphic synthesis of the Lac du Puy pedosedimentary

sequence, including stratigraphic information, radiocarbon dates, archaeological remains, and relative location of COR13-4 in the sequence.

2-Materials and Methods

Coring and pedo-sedimentary description.

Coring was performed in the basin in November 2012 following a hand auger survey, using a Geotool GTR 790 corer (diameter of 7 cm, for location see Fig. 1D). Half of the obtained 186 cm core (COR13-4) was used for palynological analysis and radiocarbon dating (see Ledger et al., 2015 for details). In the summer of 2015 geoarchaeological prospection based on geophysics and systematic trenching (Guillemoteau et al., 2016; Mayoral and Depreux, 2017; Mayoral et al., 2018) confirmed that COR13-4 was representative of the complete natural pedo-sedimentary sequence of the Lac du Puy, with limited or no truncation (Fig. 1F & G). The remaining half was used for multi-proxy geoarchaeological analyses which are described in the present study: sampling and pedosedimentary description were performed in laboratory using a Munsell color chart (see Log in Fig.2, for detailed description see Table 3 in Appendix). Detailed laboratory descriptions and macro observations were correlated with exhaustive field description of stratigraphic units and pedo-lithofacies of the basin, already established from exposures and logs (Mayoral et al., 2018).

Construction of chrono-stratigraphic framework

Radiocarbon dates from previous studies were inform the COR13-4 core and a series of stratigraphic sections across the basin (Table 1). Dates 1-6 are in COR13-4 core and dates 7-11 in a stratigraphic log in the centre of the basin (Log 4). Dates 7 and 8, taken in SU2 base (interpreted as anthropogenic backfill, see introduction), were inconsistent with the well-established typo-chronological dating of this unit (100-40 to 50-30 BCE) and were then rejected (see Mayoral et al. 2018 for details). Dates 12 and 13 were on a small ditch excavated in SU5A. Finally, dates 14-19 were at the base of storage pits

219 dug through SU5A and Weathered Basalt (WB), except date 15 which was in the infilling of a pit
220 (SU4).

221 Dated materials include bulk sediment (11 samples), macrocharcoal (>125µm, 2 samples),
222 microcharcoal (<125µm, 3 samples) and pollen (1 sample). Of the dated materials macrocharcoal can
223 be considered the most accurate, whereas microcharcoal and pollen often show larger age
224 discrepancies (relative to their stratigraphic position) owing to reworking of sediment. While bulk
225 sediment is notoriously unreliable owing to uncontrolled ageing due to the contamination by older
226 carbon (e.g. Grimm et al., 2009), but introduction of younger organic material can also distort
227 radiocarbon dates. To assess potential reservoir effects or disturbance by pedological processes
228 some of the dates were paired (dates 1-2, 3-4 and 9-10).

229 Given the scattering of dates, the possibility of sharp changes in accumulation rate and lateral
230 variability of facies, and possible contaminations or reservoir effects, we used a broad chronological
231 approach based on the assignment of radiocarbon dates to a SU, and when possible, to a part of this
232 SU (base, middle or top, see Table 1). Well-dated archaeological levels or structures with a clear
233 stratigraphic position were also used, such as archaeological layers from the Late Bronze Age 3 (950-
234 800 BCE), La Tène D1B-D2A (100-40 BCE) and La Tène D2B to Gallo-Roman (50-30 BCE) (Mayoral et
235 al., 2018). For a graphic summary of the relative stratigraphic positions of all available radiocarbon
236 dates and archaeological landmarks, see Fig. 1G.

237 The seventeen AMS radiocarbon dates where calibrated with Calib 7.0 using Intcal 13 (Stuiver and
238 Reimer, 1993; Reimer et al., 2013), and their probability distribution was plotted using CLAM
239 (Blaauw, 2010). The obtained plot was then integrated with litho-stratigraphic and archaeological
240 data following the assignment of dates to SUs. The resulting chrono-stratigraphic diagram proposes a
241 maximum age-range for each SU of COR13-4, which can be used as a robust chronological framework
242 to discuss multi-proxy data (Fig. 2).

243

Nº	Loc. (Depth / Position)	Position in SUs	Lab. code	Material	14C yr. BP	Cal. BP (2σ)	Cal. BCE/CE (2σ)
1	COR13-4 (54-57 cm)	Top of SU3	Beta-379416	Microcharcoal	2240 ± 30	2340-2155	390-205 BCE
2	COR13-4 (54-57 cm)	Top of SU3	Beta-379417	Bulk sed.	1990 ± 30	1998-1879	48 BCE-CE 71
3	COR13-4 (71-72 cm)	Top of SU4	Beta-377232	Bulk sed.	2590 ± 30	2769-2705	819-755 BCE
4	COR13-4 (71-73 cm)	Top of SU4	Beta-379418	Pollen	2750 ± 30	2894-2773	944-823 BCE
5	COR13-4 (87-88 cm)	Middle of SU4	Beta-375785	Bulk sed.	3510 ± 30	3866-3699	1916-1749 BCE
6	COR13-4 (102-103 cm)	Base of SU4	Beta-379419	Bulk sed.	3330 ± 30	3638-3478	1688-1528 BCE
7	*Log L4 (43-47 cm)*	*Base of SU2*	*Beta-434187*	*Microcharcoal*	*5550 ±40*	*6407-6289*	*4457-4339 BCE*
8	*Log L4 (43-47 cm)*	*Base of SU2*	*Beta-430610*	*Bulk sed.*	*1430 ±30*	*1375-1293*	*575-657 CE*
9	Log L4 (59-63 cm)	Base of SU3	Beta-434188	Microcharcoal	2390 ± 30	2492-2347	542-397 BCE
10	Log L4 (59-63 cm)	Base of SU3	Beta-430611	Bulk sed.	2340 ± 30	2440-2316	490-366 BCE
11	Log L4 (87-91 cm)	Base of SU4	Beta-430612	Bulk sed.	3130 ± 30	3407-3250	1457-1300 BCE
12	Ditch (base)	SU5A/WB (indet.)	Beta-418695	Macrocharcoal	5650 ± 30	6496-6344	4546-4394 BCE
13	Ditch (middle)	SU5A/WB (indet.)	Beta-418694	Macrocharcoal	5650 ± 30	6496-6344	4546-4394 BCE
14	Pit 25604 (base)	SU5A/WB (indet.)	Poz-74925	Microcharcoal	5520 ± 40	6403-6277	4453-4327 BCE
15	Pit 25604 (fill)	SU4 (indet.)	Beta-425790	Bulk sed.	3430 ± 30	3826-3593	1876-1643 BCE
16	Pit 25677 (base)	SU5A/WB (indet.)	Beta-425426	Bulk sed.	6130 ± 30	7158-6942	5208-4992 BCE
17	Pit 25703 (base)	SU5A/WB (indet.)	Beta-425787	Bulk sed.	5240 ± 30	6176-5921	4226-3971 BCE
18	Pit 25699 (base)	SU5A/WB (indet.)	Beta-425788	Bulk sed.	4780 ± 30	5591-5469	3641-3519 BCE
19	Pit 25610 (base)	SU5A/WB (indet.)	Beta-425789	Bulk sed.	5640 ± 30	6491-6322	4541-4372 BCE

Table 1. Radiocarbon database for the Lac du Puy used to build the chrono-stratigraphic framework (Fig.2), all dates have been previously published in Ledger et al. 2015 and in Mayoral et al. 2018. *Dates 7 & 8 were rejected on a stratigraphic basis (italic)*. Dates are given in BCE/CE system (Before Common Era/Common Era). Microcharcoal: <125µm, Macrocharcoal: >125µm. Dates have been placed in their stratigraphic context on Fig 1G.

Micromorphological analysis

The half-section of COR13-4 core between 40 and 144 cm was cut in 10 blocs (9 to 12.5 cm length, 7 cm width). Micromorphological thin sections were prepared from these blocks at Ghent University (B). Descriptions of thin sections from macro- to microscale were performed with a Leica M80

254 binocular microscope (x2.5 to x60), a Leica DMLP polarizing microscope (x16 to x400), and a Leica DM
255 2500M (x500). A Leica built-in camera was used to take microphotographs and measurements.
256 Minerals and alteration were identified and described following petrography references (MacKenzie
257 et al., 1982; Delvigne, 1998; Loaiza et al., 2015). Micromorphological features were semi-
258 quantitatively described and recorded, according to reference works (Bullock et al., 1985; Stoops,
259 2003; Loaiza et al., 2015; Macphail & Goldberg, 2018). Interpretation was based on international
260 standards (Nicosia and Stoops, 2017; Stoops et al., 2010a). The reconstruction of the pedo-
261 stratigraphic sequence and the pedo-sedimentary processes is based on a hierarchical approach of
262 pedofeatures (Fedoroff and Courty, 2002; Fedoroff et al., 2010).

263 ***Geochemistry and Magnetic Susceptibility***

264 The geochemistry of the COR13-4 core was analyzed using an AVAATECH XRF core-scanner at
265 EDYTEM laboratory (Université Savoie Mont-Blanc, F). The core was analyzed at a resolution of 10
266 mm under 10 Kv and 30 Kv beams generated by a rhodium anode, providing results in counts per
267 second (cps) for 24 elements. A Principal Component Analysis (PCA) was performed on selected
268 elements using XLSTAT software, in order to bring to light relationships between elements and with
269 sedimentary units of the infilling (Birks & Birks, 2006 ; Sabatier et al., 2010 ; Bajard et al., 2015). On
270 this base, elements and ratios were selected as palaeoenvironmental proxies and interpreted.

271 The Magnetic Susceptibility (MS) of the core was measured (unit: $SI.10^{-5}$) using a Bartington MS2E
272 susceptibilimeter. Four measurements were taken each cm and the mean value was retained in
273 order to integrate signal variability (Dearing, 1999). Measurements were focused on the clayey
274 sedimentary matrix avoiding coarse basaltic particles, because their strong magnetic properties
275 obscured the sedimentary signal.

3-Results

3.1-Stratigraphic Units and chrono-stratigraphic framework

Seven Stratigraphic Units (SU) were identified in COR13-4, consistent with those described in the basin infilling by previous works (see Introduction, and Fig. 1E & G; for detailed pedo-sedimentological description at the scale of the basin see also Mayoral et al., 2018). Several subunits were detected within these SU, drawing a more detailed stratigraphy for SU4, 5A, 6A and 6B (see log in Fig. 2, see also Table 3 in Appendix for detailed description of COR13-4).

The chronostratigraphic framework in Fig. 2 includes radiocarbon dates belonging to three SU (SU5A, SU4, SU3) and archaeological data at the contacts between SU4-SU3, SU3-SU2 and SU2-SU1. From these data, the chronology of SU1, SU6A and SU6B can only be estimated. Furthermore, caution must be exercised in interpreting the chronology of SU5A which was established from data drawn from multiple profiles. In the case of the Lac du Puy sequence, a reservoir effect due to old lithogenic carbon is unlikely for bulk radiocarbon samples: the geology of the basin includes exclusively volcanic materials such as basalt and scoria (Mayoral et al., 2018) which are not prone to release significant quantities of lithogenic carbon in the sedimentary environment. However, the pedogenic nature of this relatively short sedimentary sequence suggests that bulk could be subject to contamination from upper levels due to pedoturbation. From a macroscopic perspective, SU3, 4 and 5A seem not have been subject to major disturbance, but the action of rootlets, cracks due to posterior vertisolization processes or other pedogenic sedimentary inputs is not easily discernible (Mayoral et al., 2018).

A detailed analysis of the paired dates on same samples (1-2, 3-4, 9-10) shows that bulk sediment provides slightly younger ages than microcharcoal or pollen. This could be due to a limited incorporation of modern carbon from above, but microcharcoal and/or pollen could also have a small reservoir effect (Ledger et al., 2015). This is especially the case with paired dates at the top of SU3 (1-2): bulk seems slightly too young respect the corresponding archaeological landmark (100-40 BCE), whereas microcharcoal is slightly too old. When comparing other paired dates, such as at the top of

SU4 (3-4) with archaeological landmarks (950-800 BCE), it appears that both bulk and pollen dates can be considered reliable. A similar case is evident for paired dates 9-10 at the base of SU3. Bulk dates therefore appear more reliable in SU4 (massive gleysol) that in SU3 (especially towards its top), maybe due to vertisolization processes in the unit and posterior disturbance related to SU2 (Mayoral et al., 2018). Bulk dates 6 and 11 in SU4 are then considered as broadly correct.

Dates 5 and 15 are older than other SU4 dates and deserve detailed analysis: nº 5 is clearly too old considering its position at 87-88 cm in the middle of SU4 (Fig.2, Table 3). A potential cause for this would be lateral erosion of unit SU4b (see Fig 1.), bringing to the centre of the basin pedogenic materials which could include some older carbon. Date 15 corresponds to the infilling of a storage pit after its abandonment (600-425 BCE), certainly using SU4 sediment extracted when digging a new neighboring pit (Mayoral et al. 2018). In the process older or younger carbon could have been incorporated, but the date is nevertheless roughly consistent with others in SU4.

The situation is more complicated in SU5A. Here, a comparison of dates 12 and 13 (macrocharcoal) from two levels of a structure dug in this SU, with quasi-identic date 14 (microcharcoal) and slightly younger date 19 (bulk), both from adjacent levels, indicates that bulk dating is relatively accurate in SU5A. Therefore dates 16, 17 and 18 can also be considered as broadly correct. However, these dates are all situated in profiles where SU5A is in gradual transition with underlying WB, and both are almost always difficult to distinguish. Dates 16-18 therefore cannot be considered an “exact” age of SU5A, but rather provide an indicative *terminus post quem* (TPQ) and *terminus ante quem* (TAQ) for its long-term formation since first weathering stages of basaltic bedrock, a process probably initiated in early phases of the evolution of the basin from a pseudo-sinkhole (Mayoral et al., 2018).

In light of this uncertainty and the high lateral variability in stratigraphy, a direct transposition of these SU5A/WB dates to SU5A in core COR13-4 is inadvisable. Particularly given the presence of the underlying SU6A/B, which was absent in a majority of the dated profiles. Indeed, translocation of dates from elsewhere in SU5A to COR13-4 would imply ages older than 4.5-5 kyr. cal. BCE for the

lower part of the palynological sequence (see Fig. 1). This would be in marked disagreement with pollen data and with well-known regional vegetation history. Indeed, assemblages from the base of COR13-4 (Ledger et al., 2015) are clearly coherent with a landscape typical of the Mid/Late Holocene boundary in the Auvergne region, which is characterized by recognizable vegetation dynamics such as rarefaction of *Tilia* pollen frequencies, absence of *Ulmus* and increasing trends of *Abies* and *Fagus* values, amongst other significant taxa (Trément et al., 2007; Miras et al., 2018).

This apparent 2000 yr mismatch between radiocarbon dates and vegetation history is undoubtedly related to the complex chrono-stratigraphic relation between SU5A/WB and SU6A/B. These stratigraphic ensembles are at the same time in lateral transition and overlaid depending on the previous (and irregular) topography (see Fig 1). This indicates that SU5A is non-isochronous, but rather temporally- and spatially-transgressive. The development of SU5A was likely dependent on topography, in a context of differentiated micro-scale sedimentary environments in high- and low-relief areas of the basin. In this scenario, a first stage SU5A would have formed slowly on WB in higher areas, whereas SU6A/B deposited simultaneously in lower areas. In a second phase SU6A/B inputs decreased or eventually ceased, and SU5A extended to lower areas overlying them. In later stages (after SU5 deposition) the basin was leveled by sedimentary accumulation and chrono-stratigraphy becomes significantly more uniform (Fig. 1). The temporal envelope provided by radiocarbon dates in SU5/WB in high-topography areas corresponds not only to SU5A in the lower areas where COR13-4 is located, but probably also to SU6A/B.

As a consequence, the younger date obtained in SU5A (nº18) is a reliable TAQ for its deposition in both low and high areas of the basin, and also for SU6A/B. The older date obtained in SU5A (nº16) must be contemporary with the first weathering stages of basalt in high-topography areas of the basin, and is likely close to the age of the base of SU6A/B in contact with the bedrock in low-topography areas. Despite its uncertainties and limitations, this refined chrono-stratigraphic

interpretation of basal units of the pedo-sedimentary sequence satisfactorily incorporates radiocarbon, stratigraphic and palynological evidence.

Ultimately, integration of all the radiocarbon assays with archaeological data allowed to constrain the maximum age ranges for SUs 6A/B, 5A, 4 and 3 in COR 13-4 (Fig.2, down) which will be used to discuss multi-proxy data in this core. The inception of SU6A/B is unclear, although it is likely around 5200 cal. BCE. Its deposition is followed by SU5A until 3500 cal. BCE. SU4 dates range from 2000 to 800 cal. BCE approx., however considering that dates 15 and 5 could be subject of reservoir effect the interval 2000-1700 to 800 cal. BCE is proposed in order to integrate this uncertainty. SU3 age ranges from 500 cal. BCE approx. to 100-40 BCE. SU2 age, exclusively from archaeological data, is dated between 100-40 and 50-30 BCE. Two major hiatus or very slow sedimentation periods are outlined between 3500 and 2000-1700 cal. BCE, and between 800 and 500 cal. BCE.

This chrono-stratigraphic framework highlights the non-linear nature of the sedimentary chronology in COR13-4 and nuances previous age-depth model used for palynological analysis, which included only 6 dates and was very imprecise for SU5A and 6A (Ledger et al., 2015). Only minor changes affect upper units (SU2, 3, 4), which are now better constrained, especially the base of SU3 (c.500 cal. BCE, implying a short hiatus after the top of SU4) and SU4 (c. 2000-1700 cal. BCE) which are both slightly younger than previously estimated. By contrast, SU5A and SU6A/B appear slightly older (c. 5200–3500 cal. BCE). Considering this, chronology of previous data (Ledger et al., 2015; Mayoral et al., 2018) for these SUs was revised in the discussion. The apparent hiatus between 3200 and 2000-1700 cal. BCE (Fig. 2) is certainly due to a very low sedimentation phase between the top of SU5A and the base of SU4A.

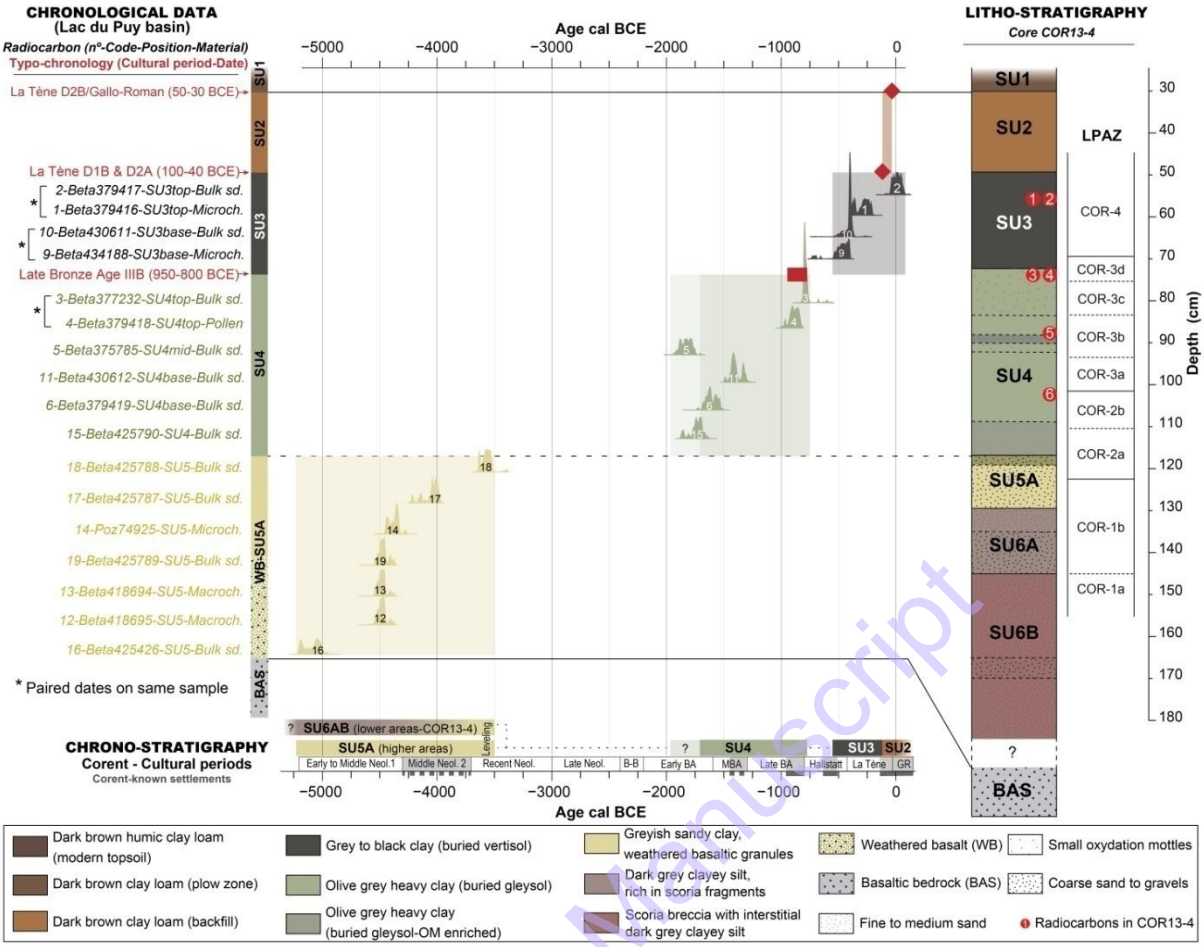

Figure 2. Chrono-Stratigraphic framework for Stratigraphic Units in COR13-4. Chronological data (probability distribution of radiocarbon dates and archaeological landmarks, left) from all the Lac du Puy basin are correlated to the Stratigraphic Units present in COR13-4 (right) and Local Pollen Assemblage Zones (LPAZ) from Ledger et al. (2015). Note that radiocarbons 1-6 are in COR13-4 itself. Relative position of dates in each SU is indicated when available (left). Dated material (bulk sediment, microcharcoal, macrocharcoal or pollen) is also noted. Red rectangle and diamonds indicate archaeological tie points. Chrono-stratigraphy resulting from the integration of dates grouped by SU and archaeological data (centre) is represented as maximum age ranges for each SU (down). Note that SU5 is not isochronous between higher and lower areas of the basin before its leveling. Note also the existence of chrono-stratigraphic hiatus or very low sedimentation phases (dotted lines). Corent chrono-cultural periods follow Poux et al., 2018 (B-B: Bell-Beaker period, MBA: Middle Bronze Age, GR: Gallo-Roman). Grey-shaded periods and grey lines indicate known settlements (dashed line: imprecise chronology or partial evidence). For detailed description of Stratigraphic Units and subunits, and archaeological data, see Table 3 (Appendix), and Mayoral et al. (2018).

386

387 3.2 Micromorphology

388

389 ***General features***

390 A detailed micromorphological description is synthetized in Table 2, and a gallery of outstanding
391 features is shown in Figs. 3 to 5. The pedosedimentary sequence of the Lac du Puy is particularly
392 complex due to the low accretion rate and the overlapping of successive pedological processes and
393 features (gleyfication, vertisolization, illuviation, weathering, etc.) since the Neolithic. The coarse
394 lithogenic fraction is strictly composed of volcanic materials such as basalt and scoria, given the
395 limited lithology of the plateau (Bouiller, 1979 ; Greffier & Restituito, 1980 ; Nehlig et al., 2003 ;
396 Mayoral et al., 2017). Chert or quartz occur as very small rock fragments (typically coarse silt to fine
397 sand fraction) and in very small quantities, and can be difficult to distinguish from small plagioclases.
398 These small lithogenic fragments are not native in the volcanic geology of the plateau, and can only
399 derive from inputs related to human activities. They are therefore considered as indicators of
400 anthropogenic influence. Micromass is composed of abundant smectitic matrix as indicated by
401 noticeable macroscopic swelling, but also clayey domains organization and a typical yellowish color
402 under microscope (Bullock et al., 1985; Loaiza et al., 2015). This matrix is often dotted with dark
403 opaque particles sometimes difficult to identify, generally magnetite and microcharcoal (<125um) or
404 small organic debris.

405 Larger organic features are uncommon and macrofaunal activity traces are extremely rare. Clusters
406 of small channels with regular diameter (100-200µm) and smooth walls, sometimes digitated or in
407 fork, are present in some layers. Studies dealing with these morphologies (Retallack, 2001; Kooistra
408 and Pulleman, 2010) allowed us to identify them as traces of rootlet mats of grasslands. Silicified
409 microfossils as phytoliths or sponge spicules (Fig. 4G) appear in some SUs: we interpreted them as
410 indicators of grasslands and wet environments respectively following literature (Gutiérrez-Castorena

411 and Effland, 2010; Vrydaghs, 2017). Masses of translucent filaments, similar to fungal hyphae but
412 much smaller (0.5µm diameter, see Fig. 3I), were identified as silicified *streptomyces*-type bacteria
413 (e.g. Néraudeau et al., 2016; Néraudeau et al., 2017). Development of these bacteria requires
414 aerobic conditions and abundant organic matter (Mayfield et al., 1972 ; Ringrose-Voase &
415 Humphreys, 1994 ; Gutiérrez-Castorena & Effland, 2010), their presence was therefore interpreted as
416 an indicator of surface horizons from a palaeosoil.

417 Pseudomorphs and alterorelics usually result from a high degree of minerals *in situ*-weathering (e.g.
418 Fig. 3) and subsequent pedoplasmation processes (Delvigne, 1998; Stoops and Schaefer, 2010). We
419 interpreted them as an indirect indicator of strong alteration processes in the soil profile due to
420 hydrological variability, drainage conditions or mechanical constraints (Fedoroff and Courty, 2002).

421 Weathering of scoria fragments in acid conditions is known to produce neoformation of aluminium
422 silicate clays such as allophane coatings (AC) and infillings. This neoformation is characteristic of
423 andic soils (Baize and Girard, 2008) and has already been described in the region (Jongmans, Van
424 Doesburgl, & Van Breement, 1990; Anthony, 1990; Jongmans et al., 1991; Ringrose-Voase &
425 Humphreys, 1994). However, the Lac du Puy pedosedimentary sequence does not include andic
426 horizons (Mayoral et al., 2018): therefore we interpreted these features (Fig. 5H and I) as inherited
427 from other soil profiles with andic features outside the basin. Additionally, small and rounded
428 fragments of clay coatings (CC) and allophane coatings (200-300µm) are present throughout the
429 sequence. Taken together, these indicators can be interpreted as evidence of the erosion of mature
430 surrounding soils with andic properties. Indeed, even clay-rich volcanic soils are especially prone to
431 runoff erosion when exposed to excessively dry or wet conditions, and especially under cultivation
432 (Legrand et al., 2007).

433 Clay translocation is quasi ubiquitous in the pedosedimentary sequence, however it is much more
434 complex in lower SUs. Various generations of clay coatings (CC) and clay infillings (CI) with different

435 characteristics can be observed (Table 2), indicating overlapping processes likely resulting from
436 successive illuviation phases under different environmental conditions.

Stratigraphic unit	Depth (cm)	CF ratio (%)	Related Distribution	Birrefringence Fabric	Microstruct.			Voids (intraped.)					Coarse Fraction							Weathering			Micro-mass		Organic Features			Pedofeatures										Description and hierarchy of textural pedofeatures
																												Redox. Features					Pedog. Aggr.					
					Primary	Secondary	Pedality dev.	Channels	Vesicles	Vughs	Basalt	Scoria	Qtz. / Plagio.	Chert	Phytoliths	Spicules	CCoats. Fgts.	A.Neof. Fgts.	Pseud. (B)	Pseud. (R)	Alterorelics	Color	Opacity	Microcharc.	Macrocharc.	Streptomyces	Fe nodules (A)	Fe hypocoats.	Fe coatings	Mn nodules	Mn coats.	FeMn nods.	Brownish (B)	Smectitic (C)	Greyish (D)	Dark Brown (E)	
2 (backfill)	**49,5-40**	25	OP	GPS/CS	SB		WA-WS	-		**	****	****	***	*	***	***						PY	****	****	**		****	***		-		*	***	-			Abundant reddish and thin CC and infillings, dusty and poorly oriented, rarely laminated
3 (vertisol)	**62-49,5**	20 to 10	OP	GPS/CS	SB	PR	WA-WS	***	-	*	***	*	***		**	**	*	**	*			PY	****	***	-		****					***	-				Abundant thin, white to orange, CC and infillings, sometimes integrated in the matrix
	73,5-62	10	OP	GPS/CS	SB	PR	WA-PS	***	-	**	***	-	-	-	****	****	*	**	-			GY	**	***	-		**	*			*	***	*	-			Abundant thin, white to orange, CC, occasionally limpid, sometimes integrated in the matrix
4 (gleysol)	**83,5-73,5**	5	OP	ST/GPS	SB		MA-MS	**	-	*	*	-	*		-	-	***	**	*			PY	*	***	-	****	***	***		*		*			***	*		Abundant thin and limpid CC, poorly oriented, sometimes integrated in the matrix
	93,5-83,5	5 to 4	VOP	GPS/ST	SB to AB	PR	MA-MS	***	**		*	-	*		**	**	***	**				YG	*	***	-	**	****		*	**		-	***				Few CC, thin and limpid
	105-93,5	4	VOP	GPS/ST	F to AB		PA-PS	****	**	**	-	-	-		-	-	**	**	-			PY	*	***	*	**	****	**	**	**		**	**	**			Very abundant whitish, thin and limpid CC and infillings, sometimes integrated in the matrix
	115-105	5 to 10	OP	GPS/ST	SB		WA-WS	**		*	**	**	-				*	***	*	****	****	PY	*	**		**	****		*	*		*	*	**			Abundant massive and thick clay infillings, quite limpid, sometimes laminated but poorly oriented

5a	**125-115**	25 to 50	OP / DSP	GPS	GR	SB	WA-PS	***	**	*	****	**	*		*	-	****	***	-	***	***	PY	*	**		-	****			**			**		**		1-Massive whitish CI, poorly oriented, between granules 2-Very abundant CC and CI whitish, in crescent, well laminated and oriented, sometimes dusty 3-Dusty brown CC in residual voids
5a - 6a	**134-125**	50	DSP / SSP	GPS	GR	SB to F	WA-PS	***	**		****	****	***	-			**	****	*	***	***	PY	**	*			**	*	*	*				****			1-Ubiquitous and massive CC and CI between granules, poorly oriented, dotted 2-Several thin CC and CI, crescent-laminated, limpid and well oriented 3-Dusty brown CC in residual voids with organic particles
6a	**144-134**	50 to 66	DSP / SSP	GPS	GR	SB to F	WA-PS	*	*	**	****	****	***	*	*			****	*	**	-	PY	**	***	**		***	***	***					****	*	1-Very abundant thin whitish CC and CI, between granules, not laminated neither oriented 2-Abundant thin whitish CC and CI, limpid and laminated, moderately oriented

Table 2. Detailed micromorphological descriptions of COR13-4. System: Stoops 2003; **CF:** Coarse-Fine (boundary fixed at 20 µm); **Related Distribution:** OP: Open Porphyric; VOP: Very Open Porphyric; DSP: Double Spaced Porphyric; SSP: Single Spaced Porphyric; **Birefringence Fabric:** GPS: Grano-Porostriated; CS: Circular Striated; ST: Striated/Strial; **Microstructure:** SB: Subangular Blocky; AB: Angular Blocky; F: Fissural; GR: Granular; PR: Prismatic; WA: Well Aggregated; WS: Well Separated; PA: Poorly Aggregated; PS: Poorly Separated; MA: Moderately Aggregated; MS: Moderately Separated; **Pedofeatures and coarse fraction:** CCoats. or CC: Clay Coatings; CI: Clay Infillings; A. Neof. : Neoformated Allophane; Frgts.: Fragments; Pedog. Aggr.: Pedogenic Aggregates; Qtz.: Quartz; Pseud. (B): Black pseudomorph; Pseudom. (R): red pseudomorph; coats.: coatings; hypocoats. : hypocoatings; Nods. : nodules; **Colors:** PY: Pale Yellow; GY: Greyish Yellow; YG: Yellowish Grey. **Abundance symbols:** no symbol: absence; - Rare; * Few; **Several; ***Abundant; ****Very abundant.

445 Iron and manganese pedofeatures are ubiquitous throughout the sequence (see Table 2, and Figs. 3
446 to 5). Each type of these features indicate different redox conditions (Kovda & Mermut, 2010 ;
447 Lindbo, Stolt, & Vepraskas, 2010), therefore we used their variability to infer redox changes in the
448 sequence.

449 Pedogenic disorthic to anorthic aggregates are also abundant in all the SUs (see Figs. 3 to 5), and can
450 be roughly grouped in five types (A,B,C,D,E) defined as following: A) Reddish nodules, impregnated
451 with Fe oxides, seem to be the result of local redox processes and can be found in all the SUs; B)
452 Large, irregular, brownish nodules, with abundant organic fragments, come likely from upper
453 superficial units, i.e. SU2 or SU1 (brown humic clay, see Fig. 2) and are translocated in underlying US3
454 and 4; C) Smectitic nodules, with abundant bright clayey domains and highly similar to SU4 matrix,
455 come certainly from this unit (SU4); D) Greyish rounded aggregates form the matrix of lower units
456 (SU5a and 6a). Their micromass, rich in microcharcoal, organic fragments and feldspar (Fig. 5)
457 suggests that they result from erosion of former organo-mineral horizons, belonging to the soils of
458 the plateau surrounding the pond. Amongst these, some (E) are particularly rich in organic micro-
459 debris and charcoal, giving them a dark brown color and a relatively humic aspect.

460 All these anorthic or disorthic pedogenic aggregates in the profile, except those from SU5A and 6A,
461 are reworked downwards due to vertisolization processes. In general terms vertisolization affects
462 SU2 to 4 as indicated by prismatic macro-structure, grano-porostriation of the fine clay matrix, mixed
463 and phytolith-rich matrix and ferromanganic nodules (Kovda and Mermut, 2010), however several
464 phases could be superimposed due to these layer-crossing processes. To disentangle this complexity
465 the established nodule types were used, as several are original from one specific layer. When
466 appearing downwards in older layers, they served as *Terminus Post Quem* for a given vertisolization
467 phase. Their vertical distribution in the profile allowed then to distinguish in relative chronological
468 order several vertisolization phases. However, when nodules appeared in levels younger than their

469 original layer, they were rather interpreted as indicators of lateral erosion from nearby areas
470 (Fedoroff et al., 2010).

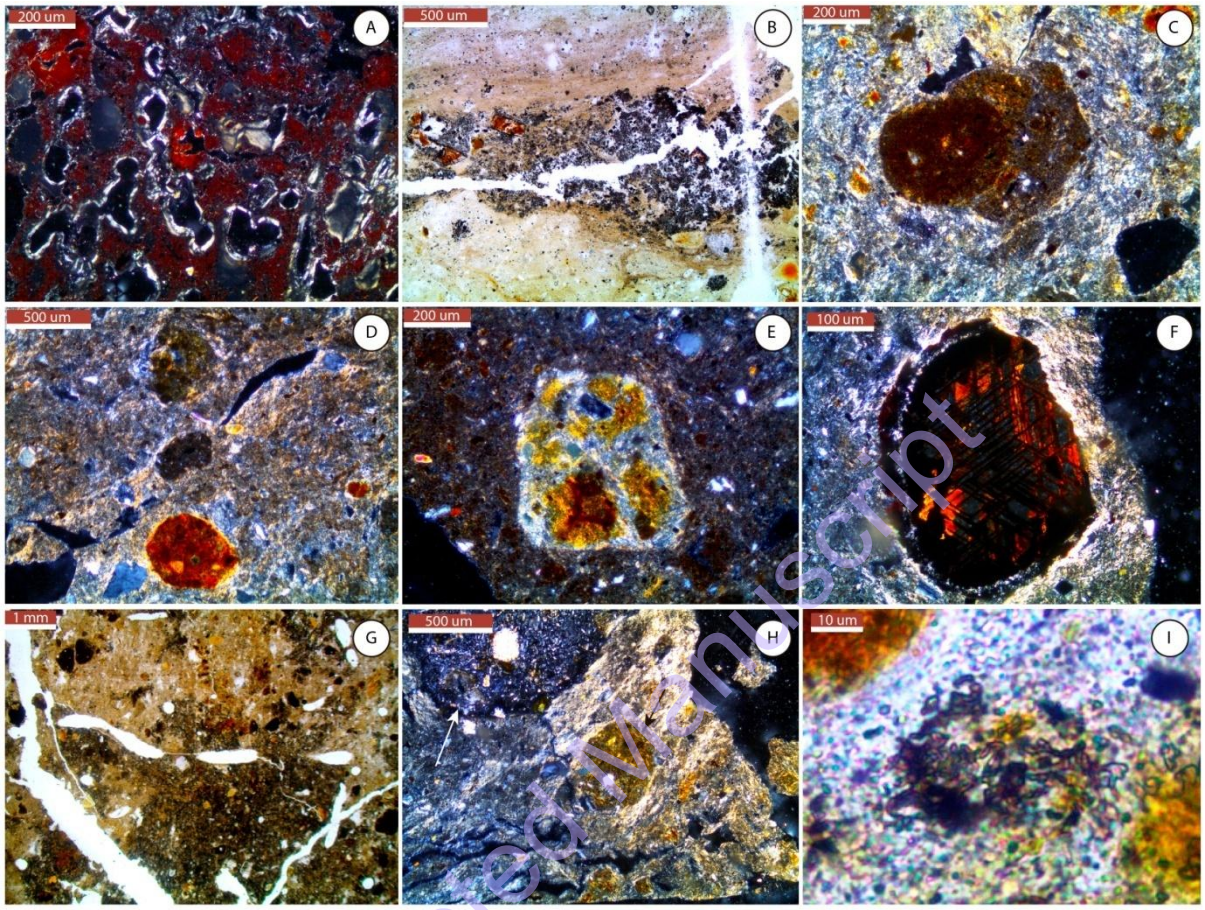

471

472 Figure 3. Micromorphological features common in all the pedosedimentary sequence of the Lac du Puy. A: scoria with
473 allophane hyaline coatings in rock vesicles. The coatings, neoformated as a weathering product, are microlaminated and
474 well oriented (SU6a, XPL). B: Black-colored scoria fragment with its left part strongly weathered, in process of
475 pedoplasmation (alterorelic). Note several pseudomorphs and an abundant clay matrix, probably in part neoformed (SU5a,
476 PPL). C: Polyphased pedogenic aggregate, made of A-type reddish nodule embedded in a B-type greyish-brown nodule,
477 both anorthic in a grano-porostriated clayey matrix (SU4, XPL). D: Variety of A- and B-type pedogenic aggregates, all
478 anorthic in a grano-porostriated clayey matrix (SU4, XPL). E: C-type smectitic aggregate from SU4, anorthic in the clayey
479 matrix of SU2 (XPL). F: Pseudomorph in *boxwork,* probably from hornblende, with strong peripheral grano-porostriation
480 (SU3, XPL). G: abundant small channels (rootlets) and dark mass composed by *streptomyces*, marking an aerobic palaeosoil
481 level (SU4, PPL). H: Basalt fragment (white arrow) and moderately iron impregned A-type nodule (black arrow), disorthic to
482 anorthic, in a grano-porostriated matrix (SU3, XPL). I: zoom into a *streptomyces* cluster, in the micromass. Note the small
483 diameter (0.5 to 1um) of filaments (SU4, PPL).

484

485

Processes and hierarchy

After identification, micromorphological features have been grouped and interpreted as processes affecting one or more SUs, and finally organized in a relative chronology based on hierarchy concept (Fedoroff et al., 2010), presented on Fig. 6.

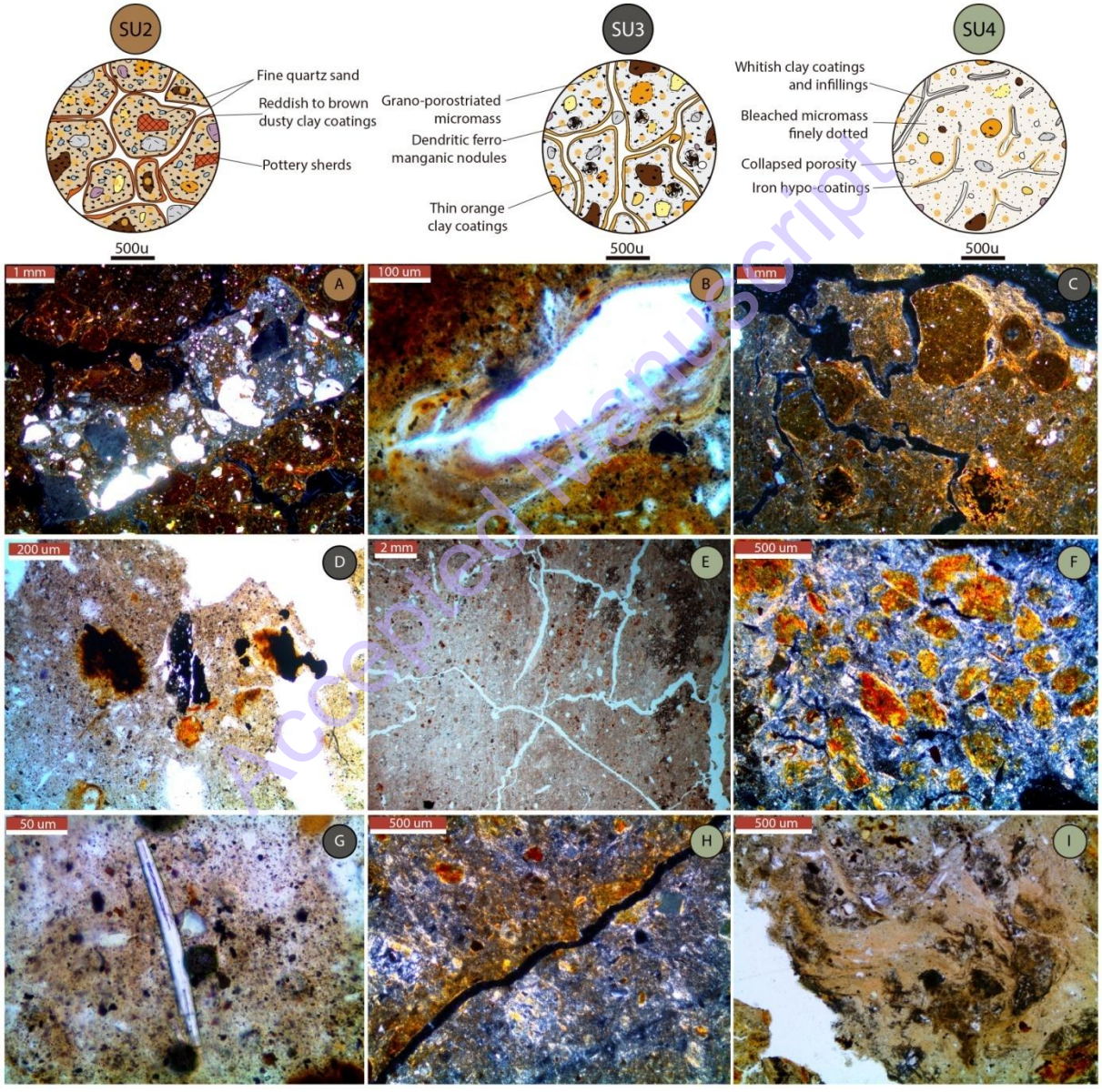

Figure 4. Micromorphological features of SU2 (brown labels), SU3 (black labels) and SU4 (green labels). A: pottery fragment, note pedogenic nodules around the fragment, the reddish thin CCs and the abundance of small feldspar or quartz crystals (SU2, XPL). B: Laminated and very dusty CC in a channel void (SU2, PPL). C: Anorthic B-type pedogenic nodules (central and upper parts of the picture) and two orthic ferromanganic nodules (lower part of the picture), with peripheral grano-porostriation (SU3, XPL). D: Macrocharcoal and ferromanganic nodules impregnated in the groundmass (SU3, PPL). E:

Blocky Angular to subangular microstructure, with poorly developed intrapedal porosity. The micromass is clayey, yellowish to grayish, dotted with organic microdebris, microcharcoal, and opaque volcanic minerals. Note also reddish Fe mottles and dark *streptomyces*-impregnated areas. (SU4, OIL). F: Iron impregnated nodules (A-type, *in situ*) in a very clayey, smectitic matrix with low first-order birefringence (SU4, XPL). G: Sponge spicule in a yellowish-grayish and densely dotted (microcharcoal, organic debris, volcanic minerals) clayey micromass (SU3, PPL). H: Diffuse iron hypocoating of a planar void. Note the clay-rich micromass with Fe mottles, bright oriented clay domains, and dotted with organic microdebris and microcharcoal. (SU4, XPL). I: massive illuviation (infillings) of the structural (inter-aggregate) porosity by fine clay (beige areas). Dark areas are *Streptomyces* masses developed on preexisting aggregates (SU4, PPL).

SU6A and SU5A

Micromorphological results show that SU5A and 6A have highly similar composition and microstructure, and are mainly differentiated by post-depositional processes. Blocky subangular microstructure, overlaid to a granular microstructure exclusively composed by stacked greyish aggregates (D- and E-type) and coarse mineral fraction (Table 2, Fig. 5) suggests soil re-aggregation after deposition of granules and coarse fraction by intense and concentrated hydrosedimentary fluxes (Fedoroff et al., 2010; Stoops et al., 2010b).

Volcanic minerals in these granules are strongly degraded (presence of pseudomorphs and hyaline allophanes), causing a differential enrichment in plagioclase probably due to long-term weathering (Delvigne, 1998 ; Stoops & Schaefer, 2010), which can be interpreted as a result of prolonged pedogenic evolution. Some of these pedogenic aggregates (E-type) have dark brown micromass, very rich in small organic fragments and microcharcoal, suggesting an origin in organo-mineral or in humic soil horizons.

With these evidences, SU6A and 5A can be interpreted as pedosediment, *i.e.* the resulting deposit of erosion of upper and middle horizons of mature andic soils from the lower and upper parts of the plateau, transported to the basin by concentrated hydro-sedimentary fluxes as small and rounded pedogenic aggregates. Erosion of these upper horizons was probably followed by dismantling of

523 deeper horizons (presence of anorthic papules in SU5A), indicating progressive erosion and land
524 degradation on the plateau.

525 Organic microparticles (mainly microcharcoal, <125u) are especially abundant in granules at the base
526 of SU6A, and are associated to macrocharcoal (>125um) which are indicative of local fires (Deák et
527 al., 2017). This, together with the presence of chert and quartz subangular microfragments at the
528 base of SU6A, indicate anthropogenic activity in these eroded soils around the basin.

529 Furthermore, the coarse fraction in SU6A and 5A shows a marked weathering gradient towards the
530 top of SU5A. Indeed, the abundant weathered scoria fragments (alterorelics) are much more
531 disaggregated and their pedoplasmation is generally more advanced upwards. This indicates that
532 deposition of pedosediment and soil re-aggregation (see above) was followed by post-depositional *in*
533 *situ*-weathering and pedoplasmation processes affecting especially SU5A and the base of SU4 (Fig. 8).
534 This evidence supports the development of a well-drained and stable palaeosoil level when
535 sedimentary inputs ceased (see also SU4 analysis below).

536 Illuviation is abundant and complex in SU6A and 5A, with three main phases (see Table 2, Fig. 6 and
537 Fig. 5B-E, G, and J-L) affecting both units. A first illuviation concerns the base of SU5A and SU6A.
538 Massive and poorly oriented CC and CI partially clogging the stacking voids of the pedosediment can
539 be interpreted as syn-sedimentary “flood coatings”. They are likely formed by a relatively fast
540 downwards translocation of the fine fraction of the hydrosedimentary fluxes which deposited the
541 granules (Brammer, 1971 ; Buurman, Jongmans, & PiPujol, 1998 ; Fedoroff & Courty, 2002 ; Kühn,
542 Aguilar, & Miedema, 2010 ; Van Vliet-Lanoë, 2010).

543 The second generation of illuvial features, with abundant thin, well-oriented and microlaminated CC
544 clog quasi completely remaining structural porosity in SU6A and especially in SU5A. Thin
545 microlaminations of CC suggest stable, well-drained soil as it occurs for example under arboreal
546 vegetation which controls illuviation (Fedoroff & Courty, 2002 ; Kühn, Aguilar, & Miedema, 2010 ;
547 Sedov, Stoops, & Shoba, 2010 ; Van Vliet-Lanoë, 2010). Therefore it can be interpreted as a palaeo-Bt

548 horizon developed mainly in SU5A. This Bt horizon could be related with overlying palaeosurface
549 horizons, as found at the base of SU4 (see
550 below).

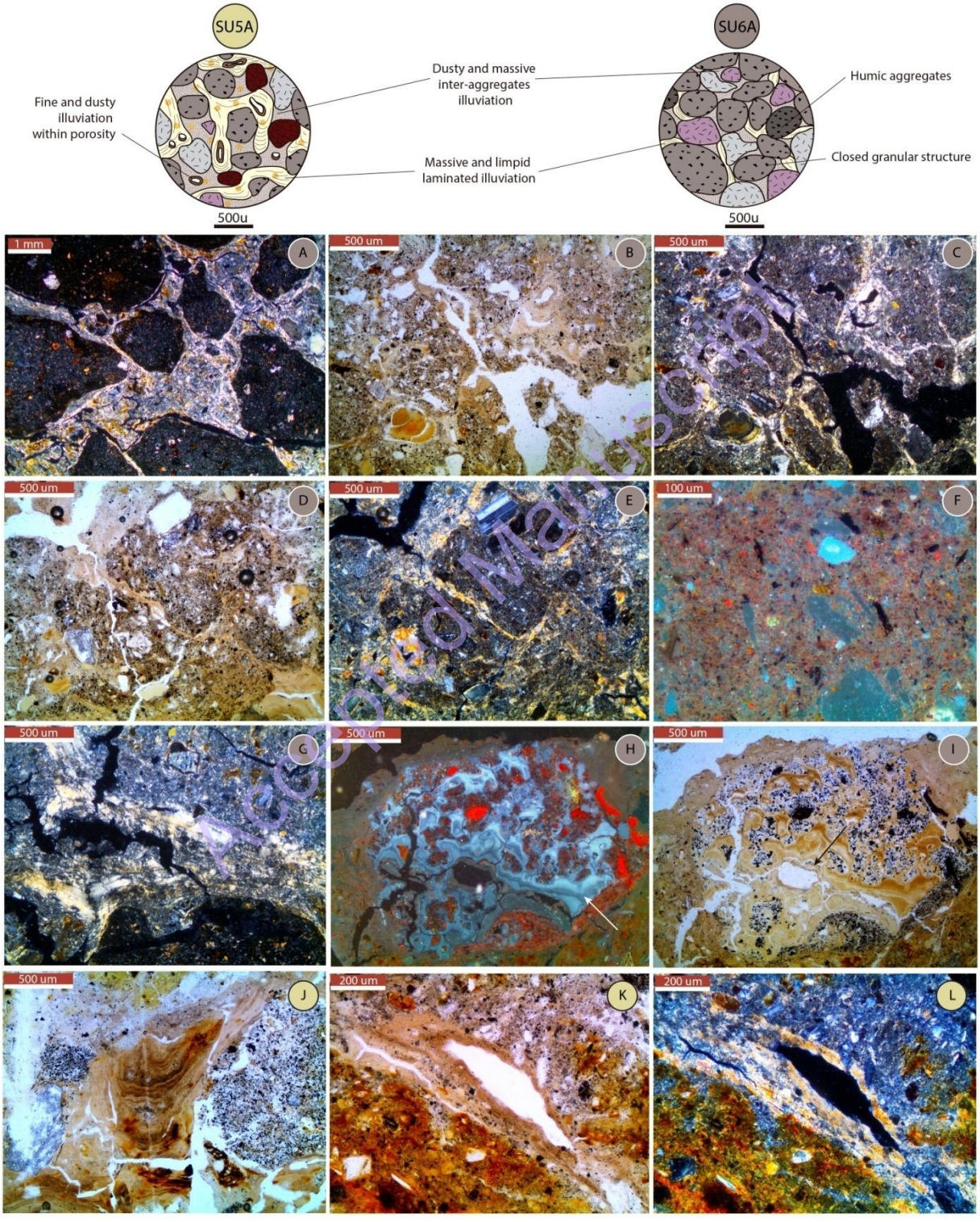

551

552 Figure 5. Micromorphological features of SU5A (yellow labels) and SU6A (purple labels). A : Basaltic coarse sand to gravel,
553 subangular to rounded, in a clayey granoporostriated matrix (SU6A, XPL). B and D: Closed granular structure, formed by D-
554 type pedogenic aggregates, and poorly separated due to posterior illuviation. Note the abundance of dark organic particles
555 in pedogenic aggregates (SU6A, PPL). C and E: same areas in XPL, note high birefringence of clay coatings and infillings, and
556 the relatively dark color of the D-type pedogenic aggregates rich in plagioclase. F: Micromass of a D-type pedogenic
557 aggregate, rich in charcoal and in small reddish particles resulting from quasi-total weathering and pedoplasmation of
558 volcanic materials (SU6A, OIL). G: Massive clayey infilling, moderately laminated, limpid and well oriented, between a basalt
559 fragment and a dark pedogenic aggregate (SU6A, XPL). H: Strongly weathered scoria granule, with reddish pseudomorphs
560 and abundant bluish-grey neoformed hyaline allophanes (white arrow) in the vacuoles (SU6A, OIL). I: same granule in PPL,
561 note opaque volcanic minerals, and fine and dusty layered illuviation in the center of the scoria fragment (black arrow) vs.
562 limpidity of surrounding hyaline allophanes. J: microlaminated coating in crescent, between several basaltic fragments.
563 Each lamination has sharper and darker base. Over imposed Fe-Mn impregnation occurs posteriorly (SU5A, PPL). K: Dark
564 and dusty clay coating in residual interstitial porosity, formed within illuvial clays between two pedogenic nodules (SU5A,
565 PPL). L: same area in XPL, note high birefringence of smectitic clays despite a poor orientation.

566 A third phase of illuviation consists in abundant thin, roughly laminated, brownish and very dusty CC
567 deposited above the textural features of the precedent phases, but also in biogenic voids developed
568 within them. These « dusty coatings » (rich in dark opaque microparticles, including microcharcoal
569 and small organic debris, e.g. Fig. 5K and L) indicate soil disturbance, even disappearance of
570 vegetation cover previously developed. They are often linked to agricultural activity (Jongerius, 1970
571 ; Macphail, Courty, & Gebhardt, 1990 ; Adderley et al., 2010 ; Kühn, Aguilar, & Miedema, 2010 ; Deák
572 et al., 2017), even if their interpretation remains complex and subject to controversy (Carter and
573 Davidson, 1998; Davidson and Carter, 1998; Macphail, 1998; Usai, 2001; Fedoroff and Courty, 2002).
574 Redox pedofeatures, mainly superimposed to illuvial features or developed in residual porosity,
575 indicate relatively important phases of water saturation (Lindbo et al., 2010) and changing
576 hydrological conditions after the last illuviation phase. This suggests a progressive drainage
577 deterioration gradually leading to typical reductic conditions.

578 ***SU4***

579 Despite apparently homogeneous conditions at macroscopic level, micromorphological
580 analysis revealed sharp vertical changes in microstructure and voids pattern throughout SU4. These
581 changes are also noticeable in groundmass, coarse fraction and pedofeatures (see Table 2). Redox

582 pedofeatures show, in general terms, absence of ferric iron and persistence of saturated reducing
583 conditions in all the SU4 (Lindbo et al., 2010), which can be interpreted as permanently high
584 groundwater level. Superimposition of textural pedofeatures shows different phases of illuviation,
585 whose characteristics (e.g. thin and limpid clay coatings) indicate that clay translocation process is
586 generally weak and slow probably under dense vegetal cover (Fedoroff and Courty, 2002; Kühn et al.,
587 2010). Based on micromorphological descriptions (Table 2), SU4 has clearly different characteristics
588 in its lower (102-115 cm), central (80-102 cm) and upper (73-80 cm) sections.

589 Microstructure and redox pedofeatures of the lower section of the SU4 (102-115 cm, see Table 2)
590 suggest weak and relatively short saturations (Fedoroff & Courty, 2002 ; Lindbo, Stolt, & Vepraskas,
591 2010 ; Stoops, Marcelino, & Mees, 2010b). This indicates a relative degradation of porosity and
592 drainage following SU5 well-drained conditions. Composition of coarse fraction (basalt and scoria)
593 suggests sedimentary inputs resulting of relatively low-intensity soil erosion affecting extensively the
594 plateau.

595 Weathering is moderate to strong in all the SU4, but is especially intense at its base (105-115 cm),
596 with abundant and very disaggregated alterorelics of scoria fragments coming from the upper slopes
597 of the plateau. This indicates very strong *in situ* chemical and/or mechanical weathering (Delvigne,
598 1998), which appears to be a layer-crossing process affecting also underlying SU5A. The advanced
599 state of pedoplasmation of these alterorelics suggests prolonged exposition to surface bio-climatic
600 agents (Fedoroff and Courty, 2002). A dense *streptomyces* mass indicates well-drained, aerobic
601 conditions. These elements support the interpretation of the base of SU4 (105-115 cm) as the upper
602 horizon of a well-drained palaeosoil level developing downwards into SU5A and 6A, which was
603 certainly allowed by less detrital and wetter conditions in the basin.

604 Massive, limpid and poorly oriented CI indicate very strong illuviation under a stable surface with
605 vegetation cover. These characteristics suggest that clay translocation may have occurred here faster
606 that in the underlying SU5A. This is probably due to runoff inputs into the basin with abundant clayey

607 suspended load, as previously described for soils subject to seasonal flooding (Brammer, 1971 ;
608 Buurman, Jongmans, & PiPujol, 1998 ; Fedoroff & Courty, 2002 ; Fedoroff, Courty, & Guo, 2010 ;
609 Kühn, Aguilar, & Miedema, 2010). This thick illuviation phase quickly causes the clogging of the
610 porosity at the base of the SU, sealing the soil profile and strongly degrading the drainage conditions.
611 This subsequently resulted in the rising of the watertable and the gleyfication of the profile: this
612 process can be understood as secondary hydromorphy (Begon and Jamagne, 1973; Jamagne, 1978).

613 Microstructure and voids in the central section of the SU4 (80 to 102 cm, Table 2) show a collapsed
614 porosity, very weak detrital inputs, and redox pedofeatures (Fe nodules, hypocoatings and coatings,
615 Mn nodules), indicating a strong and quasi-permanent saturation (Lindbo et al., 2010). This is
616 interpreted as a result of an intensification of previously started drainage degradation. The beginning
617 of wetter conditions is clearly marked by formation of several ferromanganic nodules c. 102 cm,
618 superimposed to CC of SU5A. Clay illuviation features (CC and CI) are gradually whiter, thinner and
619 less abundant upwards. These evidences support the interpretation of a microstructure closure and a
620 weakening of illuviation processes due to the installation of gleyic conditions (Fig. 8).

621 Indicators of soil erosion inputs by runoff (coarse mineral grains) also become gradually weaker in
622 central and upper parts of the SU4. An increase in the content of microcharcoal could be interpreted
623 as erosion of soils in the catchment or as local fires on grasses, however the presence of some
624 macrocharcoal (>125µm) between 93 and 102 cm, which are usually considered as local (Deák et al.,
625 2017), supports the latter hypothesis.

626 The upper section of the SU4 (72-80 cm, see Table 2) has a better developed microstructure and
627 porosity, and redox pedofeatures point to weaker and shorter periods of saturation. These features
628 indicate slightly improved drainage conditions. A slight increase in the coarse fraction suggests
629 increased runoff energy and erosion and microcharcoal is still relatively abundant. Abundant, limpid
630 but thin and poorly oriented CC are indicative of weak clay illuviation processes. A dense

631 *streptomyces* mass at the top of SU4 indicates the development of a well-drained, aerobic palaeosoil
632 level at this depth (73-85 cm) , in a similar way as in the lower section of SU4 (see above).

633

634 ***SU3***

635 The microstructure of SU3 (prismatic with grano-porostriation, see Table 2), the marked
636 weathering of an otherwise heterogeneous coarse fraction, and the presence of phytoliths
637 accompanied by sponge spicules are all indicators of highly variable hydrological inputs and intense
638 shrink-swell processes (Kovda and Mermut, 2010), which clearly denote vertisolization. Redox
639 pedofeatures such as developed dendritic Fe-Mn nodules are indicative of strong redox oscillations in
640 this SU (Kovda & Mermut, 2010 ; Lindbo, Stolt, & Vepraskas, 2010), and their distribution suggests
641 weaker saturation but more erratic hydrology towards the top of the unit. Textural features indicate
642 that illuviation is weak to moderate, and occurs probably under incomplete vegetal cover. Presence
643 of fragments of well-developed and laminated CC, abundant fragments of hyaline allophanes, some
644 smectitic C-type nodules (from SU4) and a general increase in coarse fraction towards the top of the
645 unit are all indicators of surrounding soil erosion and increasing detrital inputs. Sustained micro- and
646 macrocharcoal concentration together with a bone fragment could be indicative of human activities.
647 These data suggest a frame of generalized erosion of evolved andic soils in all the plateau including
648 the Lac du Puy itself and highly variable hydro-sedimentary conditions under human influence.

649 ***SU2***

650 This unit has an abundant and heterogeneous volcanic coarse fraction rich in feldspar,
651 including chert, pottery fragments (Fig. 4), allochtonous quartz grains and a micromass rich in
652 charcoal, which point to detrital origin under strong human influence. Abundant dusty CC and CI are
653 indicators of rapid illuviation from a bare or disturbed surface (Fedoroff & Courty, 2002 ; Fedoroff,
654 Courty, & Guo, 2010 ; Deák et al., 2017). A marked lack of biogenic voids could be indicator of surface

655 compaction and an absence of vegetation (Adderley et al., 2010 ; Deák et al., 2017). Grano-
656 porostriation of the unit and presence of sponge spicules indicate that SU2 is at some point affected
657 by temporary flooding (Kovda and Mermut, 2010; Lindbo et al., 2010), and suggests vertisolization
658 processes. Some redox features superimposed to the granular structure (Fig. 4A) indicate subsequent
659 moderate saturation phases. This unit had already been interpreted as backfill in precedent studies,
660 based on its litho-stratigraphic characteristics (see introduction, and Mayoral et al., 2018).
661 Micromorphological features indicating detrital sediment including abundant human activity
662 markers, and a bare, compacted and disturbed surface at the top of the unit, are largely consistent
663 with this previous interpretation. Moreover, they indicate a local origin of sediment from densely
664 occupied soils of the surrounding plateau, and they also outline hypothetic posterior phases of
665 flooding and saturation.

666 Despite the lack of thin sections in SU1, some of its characteristics could be inferred from available
667 data. Presence of B-type nodules (likely from SU1 and/or SU2) in SU2-3-4, and shrink-swell cracks
668 observed on the surface of the Lac du Puy basin during fieldwork, suggest that vertic processes
669 affected a part of the sequence posteriorly to SU2 deposition and until recent times (Fig 6).

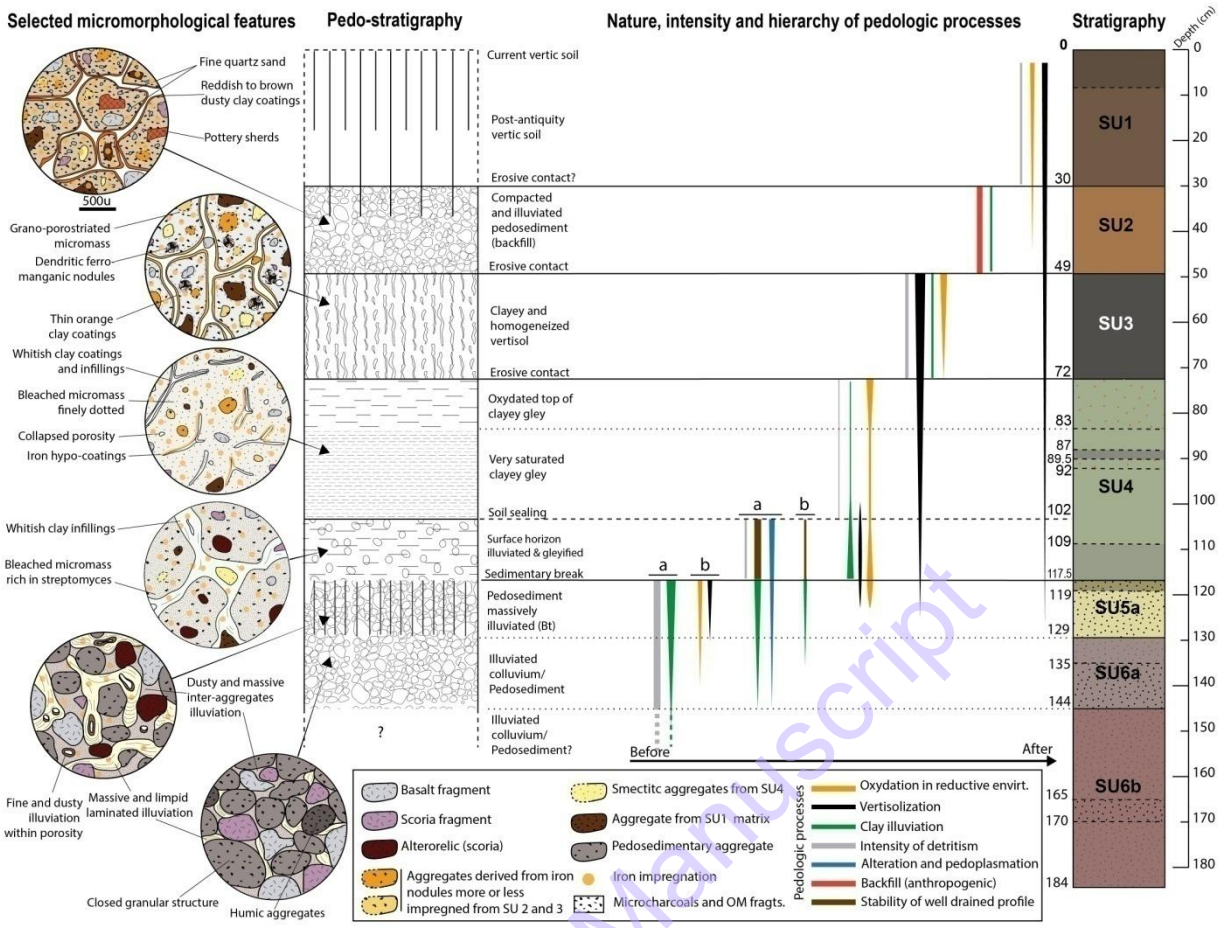

Figure 6. Pedo-stratigraphy and hierarchized interpretation of micromorphological observations of COR13-4, summarizing successive pedo-sedimentary processes distinguished in the Lac du Puy sequence.

3.3 Geochemical endmembers and selected elementary proxies

In general, the results of geochemical analysis of COR13-4 were well correlated to the different SU of the core. Nevertheless, the signal is relatively noisy due to complex pedo-sedimentary evolution of the sequence and the relatively homogeneous lithology of the plateau, making its interpretation far from straightforward. PCA shows a relatively good separation of the variables, with 70% of the variability explained by the two first components (represented by dimensions 1 and 2, Fig. 7A). Two endmembers of chemical elements can be identified, positively correlated respectively with first and second components of the PCA. The first endmember includes several lithogenic and detrital elements such as Ti, Zr, Fe, K, Si, Al, Rb and Pb, which show generally good correlation between each others in most sections of the core. The second endmember groups other elements such as Cu, Mn, Sr and Ca (Fig. 7A).

684 The distribution plot shows a relatively clear separation of the dataset by SUs (Fig. 7B). SU pedo-
685 sedimentary and micromorphological information (see previous sections) provide some clues for
686 components and related endmembers interpretation. Taking into account characteristics of SUs, the
687 primary dimension of the PCA seems to represents a gradient between lithogenic sedimentary influx
688 (positive loadings, SU3 and 4) versus pedo-sedimentary influx (negative loadings, SU6B and SU1). The
689 second dimension likely reflects finer grain-size deposits in saturated conditions (negative loadings,
690 mainly SU4), versus better drained conditions or irregular saturations with coarser grain-size of
691 deposits (positive loadings, mainly SU6B). Therefore the two endmembers represent very different
692 sedimentary inputs: elements of the first endmember are likely related to relatively fine lithogenic
693 detrital inputs, whereas elements of second endmember to coarser inputs richer in pedo-sediment.

694 Elements such as Ti, Zr, Si or Fe are lithogenic and representative of the dynamics of the first
695 endmember along the core (Fig. 7C). Zr and Ti display a very noisy signal with relatively high values at
696 the base of the core (SU6B, 6A, 5A), followed by a very sharp drop at the base of SU4. Their values
697 then exhibit less variability and are lower in this SU, but tend to increase gradually to the top of the
698 unit, and reach maximum values in SU3 before dropping again in SU2 and SU1. Zr, Ti and Fe are
699 abundant in most volcanic rocks and derived detrital materials, however Zr tends to be more
700 abundant in coarser sediment (and is often used to describe grain-size of flood layers, e.g. Corella et
701 al., 2014), whereas Ti and Fe are usually more related to fine detrital fraction (Mielke, 1979; Salminen
702 et al., 2005; Davies et al., 2015). Considering the basaltic and scoriaceous geology of the catchment
703 of the Lac du Puy, we interpret Zr, Ti and Fe as indicative of lithogenic detrital inputs, and propose to
704 use the Zr/Fe ratio as a proxy of an increase in their grain-size. This interpretation of the ratio
705 appears consistent with the grain-size observed in litho-stratigraphy (Fig. 2, Table 3).

706 Fe and Si signals are very similar to Zr and Ti (Fig. 7C), which indicates a similar relation with detrital
707 inputs. However, both show much higher relative values than Ti and Zr in units such as SU4 or SU6A,
708 suggesting sensibility to other factors. In the Lac du Puy catchment, Si results certainly from

709 weathering of basaltic rock. Colloidal Si is known to be mobile in wet, organic rich and acid
710 environments (Anthony, 1990 ; Kabata-Pendias & Pendias, 2001 ; Salminen et al., 2005). Anoxic
711 degradation of organic matter can also lead to a low pH (Osman, 2013; Blume et al., 2016), making
712 concentrations of biogenic silica more stable (e.g. phytoliths, or sponge spicules observed in thin
713 section). These considerations suggest that exceptionally high values of Si in the sequence can be
714 interpreted as a proxy of reducing conditions.

715 Fe is also a particular case, as it is an element very sensitive to redox conditions, especially mobile in
716 very wet environments (Salminen et al., 2005). This suggests that although a part of Fe in the Lac du
717 Puy is detrital, Fe concentrations are also increased in units with reducing conditions (e.g. SU4, Fig.
718 7C). Mn is also sensitive to changes in soil moisture, but is more readily mobilized in less saturated
719 conditions than Fe, and is then a good marker of oxic conditions (Lindbo et al., 2010; Kylander et al.,
720 2011). The very sharp peaks in SU3 (Fig. 7C), a unit characterized by vertic processes, suggest that
721 high Mn values can be due to ephemeral flood and drying cycles. However, as Mn can also be of
722 lithogenic origin, we propose to use Mn/Ti ratio to discriminate this hydrological signal.

723 Furthermore, given the opposite sensitivity to redox conditions in the Lac du Puy of Fe and Mn, their
724 ratio could therefore be a proxy very sensitive to redox variability and especially the intensity of
725 reducing conditions (e.g. Haberzettl et al., 2007; Cuven et al., 2011; Corella et al., 2012), which
726 appears consistent with previous litho-stratigraphic and micromorphological observations.

727 Ca variability provides information of the dynamics of the second endmember: its values are
728 especially high at the base of SU6B, and then gradually decrease upwards in SU6A and 5A (Fig. 7C). A
729 drop is also clearly visible at the base of SU4, followed by slowly and regularly increasing values from
730 SU4 to SU1. In volcanic contexts, Ca often derives from the chemical weathering of plagioclases
731 (Wedepohl, 1978 ; Mielke, 1979 ; Salminen et al., 2005). This process can result in relative Ca-
732 enrichment of volcanic soils (Kabata-Pendias & Pendias, 2001 ; Salminen et al., 2005). At the scale of
733 the basaltic plateau of Corent, we propose to interpret high Ca values of soils as the result of their

734 long-term evolution under relatively moist conditions facilitating weathering, *versus* raw detrital
735 products richer in Fe or Ti. In the Lac du Puy basin, we can therefore interpret that high Ca/Fe ratio
736 values indicate predominantly pedogenic instead of lithogenic sedimentary inputs. This
737 interpretation is clearly supported by higher values of Ca and Ca/Fe in SU5A and 6A-B (Fig. 7C),
738 where micromorphological analysis revealed abundant pedosediment (see 3.2.). Ca/Fe can hence be
739 seen as an indicator of soil erosion in the plateau (especially if it covariates with other proxies of
740 detrital inputs), however it could also indicate *in situ* pedogenetic processes.

741 Finally MS (see Fig. 7C), a measurement sensitive to magnetization, can be sensitive to different
742 natural processes including soil genesis, fires, detrital influx or volcanic fallouts (Dearing, 1999; Dalan,
743 2017). In the basaltic context of the Lac du Puy, MS signal is likely sensitive to fine detrital influx
744 (partly obscured by coarse fraction rich in magnetite grains). However, given high values in SU5A and
745 base of SU4A, it could also be indicating pedogenic sediment influx and/or local soil genesis. MS can
746 hence be combined with Zr/Fe and Ca/Fe to interpret complex processes where detrital lithogenic
747 inputs of variable grain-size, pedosediment influx and local soil genesis are entangled.

748 Following the interpretations and proposed elementary ratios developed above, a clear
749 differentiation between SUs can be detected, indicating broadly different environmental dynamics
750 between lower (SU5A and 6A/B), middle (SU4 and 3) and upper (SU2 and 1) sections of the sequence
751 (Fig. 7C).

752 Pedogenic inputs are high (Ca/Fe) but diminishing upwards in SU6A and 6B, as shown by
753 micromorphological analysis. Relatively dry conditions seem permanent through the SU (Fe/Mn,
754 Mn/Ti). MS increase and lower values of Zr/Fe and Ca/Fe in SU6A suggest less pedosedimentary and
755 more lithogenic inputs in the basin, in slightly wetter conditions (higher Fe/Mn and Si). However, the
756 highly detrital nature of the unit demands caution in data interpretation. SU5A and the base of SU4
757 show stronger lithogenic detrital inputs and pedogenic influx signal (high MS, Zr/Fe, Ca/Fe). This is
758 roughly consistent with detrital inputs followed by pedogenesis and Bt horizon formation shown by

759 micromorphological analysis (see 3.2). Changing redox conditions suggest a relatively dry phase
760 followed by wetter conditions from the top of SU5A (sharp increase of Fe/Mn and fall of Mn/Ti c. 120
761 cm), also consistent with litho-stratigraphic and micromorphological data.

762 In the middle and upper part of SU4, geochemical proxies show a clear break: ratios indicating
763 lithogenic and pedogenic detrital inputs fall dramatically and remain quasi-stable, with only a faint
764 increase towards the top of the SU, and the fine fraction becomes dominant (low Ca/Fe, Zr/Fe, and
765 MS). Hydrological conditions become highly and quasi-permanently saturated (Fe/Mn, Mn/Ti), and
766 reductic (gleyic) processes broadly dominate save for two short slightly drier phases, one intercalated
767 in the middle-upper section of the SU (92-86 cm approx.) and the other at its top (75-72 cm),
768 associated with minor detrital pulses. Lithogenic and pedogenic detrital inputs increase sharply at the
769 transition to SU3 (Zr, Ti, Ca/Fe, Zr/Fe, MS), and continue to rise gradually upwards. The general trend
770 towards less reducing (drier) conditions is punctuated by very sharp drying episodes recorded in the
771 upper part of the unit (peaks of Mn/Ti), consistent with recurrent seasonal flooding and
772 vertisolization observed in thin section (see 3.2). Geochemical data are lacking for SU2, and SU1
773 represents subactual to actual pedo-sedimentary dynamics.

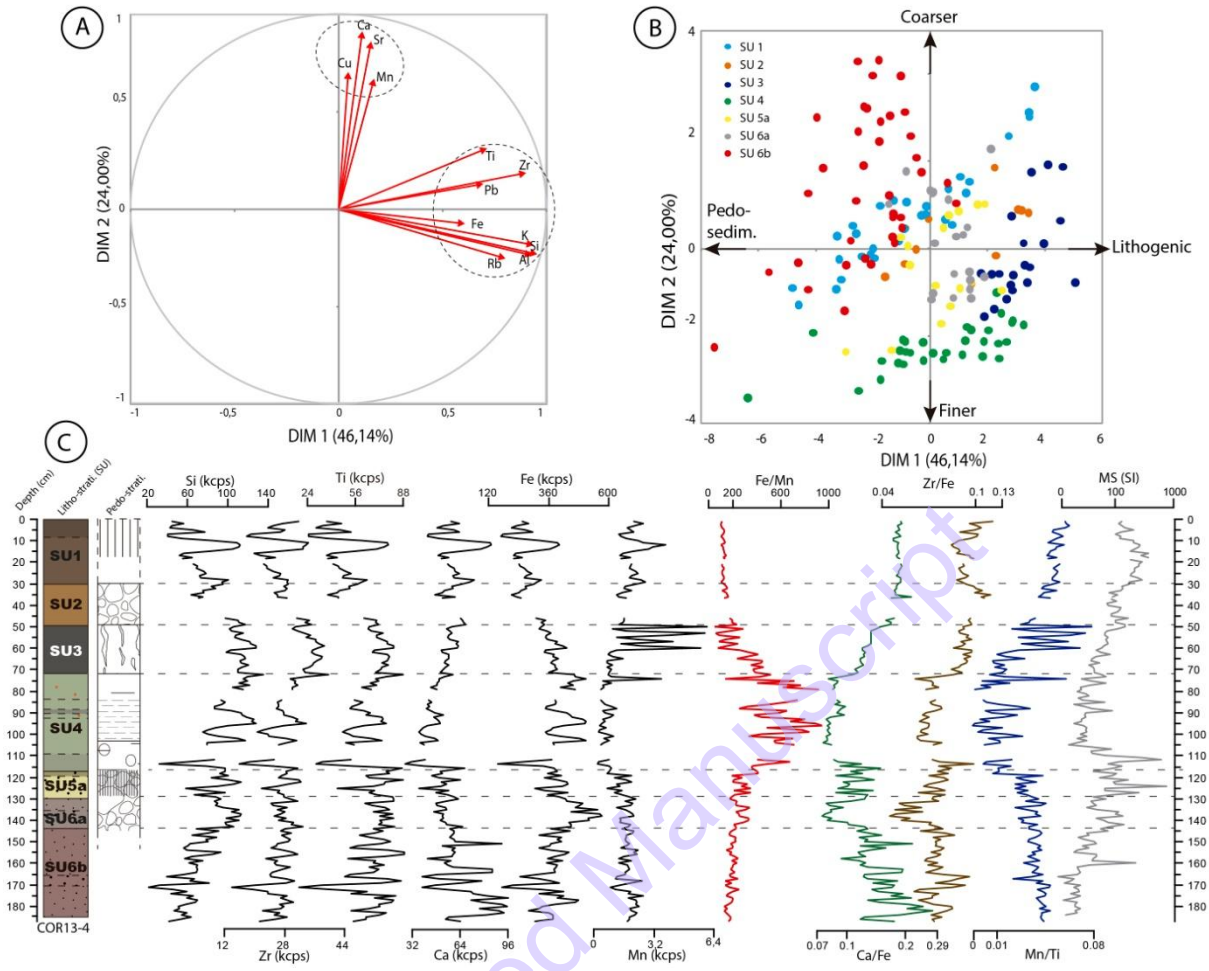

Figure 7. Selected geochemical results of COR13-4. A) PCA correlation circle according to dimensions 1 and 2 and identified endmembers. B) Plot with SU distribution C) detailed geochemical diagram of COR13-4 with selected elements and elementary ratios selected as environmental proxies. MS values are in SI (10^{-5}) and XRF values in counts per second (CPS). Ratios are dimensionless.

4-Discussion

4.1 The Early and Middle Neolithic (Mid-Holocene period)

SU6A/B and SU5A likely date to the late Early and Middle Neolithic period (c. 5200-3500 cal. BCE, Fig. 8). The period from the base of SU6B is characterized by marked detrital influx including abundant scoria and pedological aggregates, suggesting significant erosion across the plateau. The lack of palynological and micromorphological data, as well as chronological data limits interpretation for this period, which is based on geochemical and sedimentological proxies. Detrital influx increases toward the top of SU6B accompanied by slightly moister conditions. However, the pedogenic fraction is less abundant suggesting that mature andic soils of the plateau were gradually eroded and replaced by younger, more lithogenic materials.

Numerous proxies (Ca/Fe and Zr/Fe ratios, MS in Fig. 8) suggest a second phase characterized by a slight reduction in soil erosion and detrital inputs (SU6A) accompanied by a minor increase in moisture (Fe/Mn, Mn/Ti). Micromorphology indicates recurrent flooding of the basin due to intense hydro-sedimentary fluxes from the plateau. These inputs, rich in detritic and pedogenic elements embedded in fine clayey matrix, imply that despite a relative lull the erosion of soils of the plateau remains intense. The presence of allochtonous microfragments of chert and quartz, accompanied by micro and macrocharcoal indicate anthropogenic activity close to the basin. Palynological data (Fig. 8) indicate the possibility of local cereal cultivation associated with an opening of the local pine woodlands, which were developed around the depositional basin, from the beginning of SU6A as shown by lower half of LPAZ (Local Pollen Assemblage Zone) COR-1b (Ledger et al., 2015).

The end of the period (SU5A) is characterized by renewed soil erosion (higher values of Ca/Fe, Zr/Fe, MS and *Glomus*), also evidenced by micromorphological analyses (abundant pedo-sedimentary

aggregates). This suggests an increase of the anthropogenic impact on soils. Palynological data indicate an intensification of woodland clearance (decrease of arboreal pollen, increase of Poaceae) perhaps associated with pastoralism (presence of coprophilous fungi), corresponding to the upper half of LPAZ COR-1b and start of COR-2a (Ledger et al., 2015, see Fig. 8).

These geoarchaeological and palaeonvironmental data reflect a more or less continuous impact on soils and maintained erosion during the Late Early and Middle Neolithic. The opening of its first phase (SU6B) c. 5200 cal. BCE fits well with the earliest evidences of Neolithic activity at Corent (5200 to 4300 BCE, Poux et al., 2018), and suggests soils of the plateau were affected by human activities from their beginning. During later phases (SU6A, 5A), micromorphological and palynological data indicate that soil erosion and detrital inputs are more certainly linked with human activities such as forest clearance and agropastoralism. The two separated episodes of impact on vegetation detected by previous palynological study (Ledger et al., 2015) become here more clearly differentiated as they roughly correspond to SU6A and SU5A. Due to chronological uncertainties, it is difficult to say if the first is associated with Early or Middle Neolithic impacts. However, the second and more intense impact episode affecting vegetation and soils (SU5A) seems more clearly related to the Middle Neolithic fortified camp dated 4200-3700 BCE approx. (Poux et al., 2016, 2018). This latter phase can be seen as the culmination of long-term environmental impact history started in the Early Neolithic.

4.2 Recent to Late Neolithic and transition to Early Bronze Age (Middle to Late Holocene shift)

The period covering Recent to Late Neolithic and the transition to the Early Bronze Age corresponds to the base of SU4 in the COR13-4 sequence, between 117,5 and 102 cm approx. (c. 3500 to 2000-1700 cal. BCE, see Fig. 8). Two different phases can be distinguished within this relatively short core

832 section. In its lower half, micromorphological and litho-stratigraphic data show increased landscape
833 stability, however geochemical data temper this interpretation, suggesting continued mineral and
834 pedogenic detrital inputs (MS, Ca/Fe, Zr/Fe, *Glomus*) while soil hydrological conditions become more
835 saturated (Fe/Mn, Mn/Ti, Fig. 8). Palynological data point to continued opening of the landscape and
836 general disturbance (peak of Poaceae and presence of apophytes; end of COR-2a in Fig. 8, see also
837 Ledger et al., 2015). Relatively mild climatic conditions prevailed during the Recent and Late Neolithic
838 in Western Europe, although bounded by two Rapid Climate Change periods of 5.6-5.3 and 4.2-3.9
839 kyr. cal. BP (Mayewski et al., 2004; Magny et al., 2006; Wang et al., 2013; Carozza et al., 2015). Thus,
840 increased saturation of the basins soils was unlikely to have been climatically driven, but rather a
841 result of gradual soil profile sealing and slight drainage deterioration due to sedimentary
842 accumulation.

843 The upper half of the 117.5-102 section shows clearly different dynamics. Despite a data hiatus,
844 geochemical and sedimentological proxies (MS, Zr/Fe, Ca/Fe, Fig. 8) indicate reduced lithogenic and
845 pedogenic detrital inputs. This decrease is also supported by a reduction in the content of *Glomus*
846 fungal spores, which are indicative of soil erosion (Ledger et al. 2015). Soil saturation remains
847 moderate and comparable to the previous period. Micromorphological analysis revealed that this
848 phase corresponds to the development of a well-drained palaeosoil (top of surface horizon c. 102
849 cm, Fig. 6 and Fig. 8) certainly under vegetal cover, consistent with palynological data which indicate
850 local pine and oak woodlands recovery and decline of human activity suggested by the fall of
851 Poaceae and apophytes (LPAZ COR-2b in Fig.8, see also Ledger et al., 2015). The high degree of
852 weathering of coarse fraction in the profile of this palaeosoil, and the well-developed clay illuviation
853 features below its upper horizon (see Fig. 6) are traits usually needing several centuries or even
854 millennia to develop (Courty & Fedoroff, 2002 ; Fedoroff & Courty, 2002 ; Kühn, Aguilar, & Miedema,
855 2010). This strongly suggests that this palaeosoil remained stable (and so the surrounding
856 environmental conditions) over a long period, implying a marked demise of anthropogenic impact in
857 the Lac du Puy and in the surrounding plateau. This palaeosoil is also crucial to understand the basin

chrono-stratigraphy, as it explains the almost negligible sedimentary accretion between the top of SU5A and the base of SU4 (3500-2000/1700 cal. BCE). Hence, the Recent and Late Neolithic are represented in the sequence by only a few centimeters, and SU4 truly starts at 102 cm, c. 2000/1700 cal. BCE (see Fig. 8).

Geoarchaeological and palaeoenvironmental data show a clear trend towards a decreased human activity and reduced impact on palaeoenvironments between 3500 and 2000/1700 cal. BCE. A first phase of apparent stabilization and incipient slowdown is followed by a second and prolonged phase of more marked demise with vegetation recovery, reduced sedimentary accretion and soil stabilization in the Lac du Puy, indicating a long period of very limited soil erosion of the plateau. This two-phased pattern of decreasing human influence on environments appears consistent with the archaeological record. During the Recent Neolithic (3700-3000 BCE) signs of occupation at Corent are limited. However significant environmental impacts are recorded in COR13-4, suggesting archaeological data may be underestimating human activity from this period. Our knowledge of human activities at Corent during the Late Neolithic comprises a collective burial in the summit of the plateau (Daugas, 1972; Milcent et al., 2014b; Poux et al., 2018), roughly dated c. 3000-2400 BCE. After this, archaeological data become scarcer as the site is all but abandoned from the end of the Bell-Beaker period (c. 2400-2200 BCE), until the first centuries of the Bronze Age (Poux et al., 2018). The rather warm and dry climate of the Middle Holocene period prior to the 4.2 kyr BP climatic event (Wanner et al., 2008; Carozza et al., 2015; Bini et al., 2019; Cartier et al., 2019), suggests that the primary cause of this marked abandonment has to be found in social dynamics (e.g. local changes in settlement pattern), perhaps combined with pronounced andic soils deterioration after centuries of strong soil erosion due to anthropogenic activities.

4.3 The Bronze Age

Central and upper sections of SU4 (102-83 and 83-72 cm respectively in COR13-4) broadly correspond to the Bronze Age (BA), perhaps excepting its first centuries (2000/1700 to 800 cal. BCE

883 approx.). The distribution of radiocarbon dates on COR13-4 (Fig.2 and Table 1) indicates that central
884 section of SU4 represents likely end of Early and Middle Bronze Age, whereas upper section of the
885 unit records roughly the Late Bronze Age.

886 From the opening of central section of SU4 (102-83 cm in COR13-4, Early to Middle Bronze Age)
887 major hydro-sedimentary changes occur: sedimentary inputs become dominated by the clayey
888 fraction, and water saturation of the soils of the basin becomes permanent (high Fe/Mn, low Mn/Ti
889 in Fig. 8). Despite the apparently low activity of sediment transport indicators (MS, Zr/Fe, *Glomus*),
890 micromorphological analysis indicates sedimentary sources extended through the plateau. This
891 suggests generalized erosion requiring, paradoxically, increased energy to ensure sedimentary
892 connectivity and sedimentary transfer from upper to lower areas of the plateau. Micromorphological
893 features also indicate sudden changes affecting soils of the basin (dusty coatings, macrocharcoal),
894 likely anthropogenic disturbance of soils, land clearing and local fires (Deák et al., 2017). Towards the
895 top of the central section of SU4, micromorphology and geochemistry suggest that reductic
896 conditions decrease with more irregular and oscillating water saturation (Fe/Mn, Mn/Ti, Fig. 8), and
897 a slight increase of detrital inputs intensity (MS, Zr/Fe, Ca/Fe).

898 Palynological data from previous studies indicate here a second significant episode of woodland
899 clearance (Arboreal Pollen (AP) falls to minimum values, Fig. 8) probably fire-induced (substantial rise
900 of microcharcoal concentrations throughout the SU) and evidences of an arable and pastoral
901 agriculture (maximum values of Cerealia pollen-types, pollen evidences from weeds, significant rise
902 of coprophilous fungi, see LPAZ COR-3a in Fig. 8, and also Ledger et al., 2015). Towards the end of the
903 phase, pronounced landscape opening after a minor woodland recovery and sustained agricultural
904 activity (continuous presence of cereal pollen type) are accompanied by a minor microcharcoal peak
905 (LPAZ COR-3b in Ledger et al., 2015).

906 Geoarchaeological and palaeoenvironmental indicators co-variation suggests that human activity
907 increased at Corent during the end of Early and Middle BA: this situation runs contrary to the

908 regional pattern for this period, where climatic deterioration (Burga et al., 2001; Siklosy et al., 2007;
909 Gauthier et al., 2008; Magny et al., 2009) seems contemporaneous to a marked cultural decline and
910 re-location of sites in peripheral areas respect to the previous settlements (e.g. Berger et al., 2007;
911 Pétrequin and Weller, 2007; Milcent et al., 2014b). Understanding the reasons for these particular
912 dynamics at Corent, perhaps related to its hilltop situation, would require more robust archaeological
913 and palaeoenvironmental data at the scale of the southern Limagne region.

914 The discrepancy between probable important impacts on soils across the plateau and extremely low-
915 energy hydrosedimentary signal in the Lac du Puy, which persists in all the SU4, is another major
916 issue raised by our results. It can only be explained by a constrained sedimentary connectivity, i.e.
917 restricted to finer particles. A hedge-type structure bordering the basin, linked to specific pastoral
918 land use of this wet area is therefore plausible, perhaps similar to the current situation. It is
919 worthwhile noting that it is also during the BA when the first traces of agricultural plots demarcations
920 are noted in France (Carozza et al., 2007). Even a simple vegetal structure can have efficiently
921 filtered hydrosedimentary inputs into the basin (Rey, 2005). It likely caused that exclusively fine
922 suspended load supplied the basin, despite probable intensive impacts on surrounding soils and
923 enhanced erosion and runoff. However contribution of other factors to this buffering, such as
924 improved agropastoral management (e.g. reduced splash erosion on grasslands) since the Late
925 Neolithic (Barker, 1985 ; Rösch, 1998, 2013) cannot be excluded.

926 These hydrosedimentary inputs rich in fine fraction are also presumably the cause of soil porosity
927 clogging shown by micromorphological analysis. Clays deposited in the basin were probably also
928 illuviated into underlying soil porosity, already partly obstructed by previous illuviation phases (see
929 4.1 and 4.2). The consistent rise of microscopic charcoal from the base of SU4 (Fig. 8) and
930 micromorphological evidence of local fires (macrocharcoal) indicate that burning was probably used
931 to maintain open grasslands for agro-pastoral activity in the basin, a practice whose efficiency is
932 attested by experimental archaeology (Pavelka et al., 2017). This kind of management could have

933 favored clay illuviation (Slager & van de Wetering, 1977 ; Huisman et al., 2012 ; Deák et al., 2017).
934 This certainly resulted in complete obstruction and collapse of soil porosity, drainage deterioration,
935 and subsequent development of vertic conditions, quickly followed by true reductic, permanently
936 saturated conditions. Hence, our data suggest that agropastoral management practices since the end
937 of Early BA have indirectly but strongly contributed to the sealing of the soil profile and provoked a
938 marked change in environmental conditions in the basin. Increasingly wetter conditions could have
939 encouraged this kind of pastoral management, then generating a feedback effect.

940 In the upper section of SU4 (83-72 cm in COR13-4, Late Bronze Age, Fig. 2 & 8) micromorphology and
941 geochemistry indicate similar dynamics to previous phase. It is first characterized by very weak
942 detrital inputs and marked reductic conditions. Palynological data continues to depict a very open
943 and cultivated landscape as suggested by lowest values for woodland pollen and maximal values of
944 cereal and Poaceae pollen types (LPAZ COR-3c in Ledger et al., 2015). However, at the end of this
945 phase (Late BA3, 9th century BCE) indicators are again similar to the top of central section of SU4,
946 with suddenly drier conditions and slightly higher detrital inputs, but also biological activity on stable
947 and aerobic soils revealed by micromorphology (see 3.2). Palynology notes a slight woodland
948 increase, agricultural practices are less intensive or are more distant from the Lac du Puy basin, and
949 pastoralism markers such as coprophilous fungi slightly increase, suggesting the local presence of
950 livestock in the basin (LPAZ COR-3d in Ledger et al., 2015).

951 Therefore, two similar cycles of palaeoenvironmental impact can be distinguished during the BA,
952 despite a relatively imprecise chronology. The first one (central section of SU4, 102-83 cm in COR13-
953 4) covers likely the end of Early and Middle Bronze Age, and the second one the Late Bronze Age.
954 Both start with impacts linked to pastoral and arable agriculture, while archaeological traces of
955 human activity remain weak for these periods (Milcent et al., 2014b ; Poux et al., 2018). Then,
956 impacts on the basin increase with a roughly similar signature (dryer conditions, increased detrital
957 inputs), during the end of the Middle Bronze Age (c. 1450-1300 BCE), and more clearly in the Late

Bronze Age 3 (950-800 BCE). Situation of the end of LBA has been connected with extensive and dense settlement developed in the plateau, including an extended archaeological layer in the centre of the Lac du Puy (Milcent et al., 2014a; Ledger et al., 2015; Mayoral et al., 2018). Considering that environmental conditions of the basin appear dependent on human activity, these parallel impact signatures allow proposing that relatively large settlement on the plateau perhaps developed during the end of the Middle BA. This hypothesis suggested by our results is also supported by recent archaeological finds suggesting a hitherto underestimated scale of settlement in the middle BA at Corent, even if the period remains poorly known (Poux et al., 2018). This highlights how palaeoenvironmental studies in "site-proximal" contexts can efficiently complement more classical archaeological approaches.

4.4 The Iron Age and the Romanization

The Iron Age approximately corresponds to SU3 in COR13-4 (Fig. 8). However, radiocarbon probability distribution associated with results from previous works (Fig. 2) are indicative of a hiatus in the pedo-sedimentary sequence. This encompasses most of the Hallstatt period, and is associated with the construction of a battery of storage pits (c. 1000 structures estimated) in the VIth or Vth century cal. BCE (Mayoral et al., 2018). Sedimentary accumulation restarted only after this disturbance of the basin. Therefore SU3 records only the end of the Hallstatt and La Tène periods (500 to 100-40 cal. BCE aprox.). Additionally, the low chronological resolution, poor quality and homogenization of the sedimentary signal (see 3.2), together with anthropogenic destabilization of hydrosedimentary functioning of the basin associated with the pits excavation (Mayoral et al., 2018) imposes caution on interpretation. In general terms, sedimentological and micromorphological data (see 3.2) suggest a strong increase in discontinuous hydrosedimentary detrital inputs arriving into the

basin. Considering the maturity of observed vertic pedofeatures of SU3 (Kovda and Mermut, 2010), active vertisolization due to these discontinuous inputs occurred for at least four to five centuries.

Two phases with different trends can nevertheless be distinguished in SU3. The first one starts from the base of the SU: the geochemical signal becomes much more detrital than in SU4, and richer in the pedogenic fraction (higher values of MS, Zr/Fe, Ca/Fe, Fig. 8). Chemical proxies indicative of redox (Fe/Mn, Mn/Ti) suggest generally drier and less saturated conditions than in previous phases. Palynological data point to a slight vegetation recovery despite continued evidence of anthropogenic activity such as microcharcoal or pollen of disturbance-related plants. However, strong post-depositional disturbances such as marked erosion or seasonal flooding indicated by increased records of algal spores of *Zygnema*-type (and also supported by presence of sponge spicules, see 3.2) make interpretation complex (LPAZ COR-4 in Ledger et al., 2015). Suddenly increased hydrosedimentary activity, soil erosion and intermittent hydrology from our results can be considered as specific environmental consequences of strong disturbance induced by Hallstatt settlement and battery of storage pits excavation, followed by their rapid abandonment (Mayoral et al., 2018). In addition, the abundance of microcharcoal at the base of SU3 noted both by palynology and micromorphology (Fig. 8, Table 2) can be interpreted as traces of dismantling of first Iron Age soils from the archaeological site, likely destroyed by fire (Milcent et al., 2014b). Anthropogenic pressure weakens during this period, consistent with partial site abandonment during late Hallstatt and early La Tène periods (Poux et al., 2018). However, the persistence of these hydrosedimentary dynamics over several centuries suggests a relative continuity of human impacts on soils.

In a second phase, detrital fluxes intensify towards the top of SU3 including coarser particles and pedogenic fractions coming from distant areas of the plateau, indicating intense and widespread soil erosion (high values of MS, Zr/Fe, Ca/Fe, *Glomus* fungal spores, microcharcoal, fragments of textural pedofeatures and scoria fragments). Some markers of human activity such as bone or pottery fragments (see Fig. 4) appear for the first time in the sequence. Micromorphology and geochemical

proxies suggest short and violent cycles of saturation (flooding) and drying of soils. Intensified and extended erosion processes and irregular hydro-sedimentary activity are indicative of renewed anthropogenic disturbance and intensified impacts on soils and hydrology. This signal is consistent with the gradual emergence of the huge Gallic *oppidum* covering the entirety of the plateau towards the end of the Iron Age (Poux, 2012). Surprisingly, only the margins of the Lac du Puy are occupied during this period (Mayoral et al., 2018). Geoarchaeological results from this study suggest that the basin probably formed part of the sanitation/drainage system of the *oppidum*. At this time, the Lac du Puy was a marginal occupation zone, affected by repeated concentration of hydro-sedimentary fluxes caused by increased runoff and erosion, likely related to increased sedimentary connectivity and massive soil disturbance and artificialization in the plateau.

Interpretation of environmental dynamics in SU2 (dated 100-40 to 50-30 cal. BCE) is hindered by a gap in geochemical data, which only permits us to speculate on generally drier conditions and increased pedogenic inputs than in the preceding phase (Fig. 8). Micromorphology depicts a rather dry, compacted and bare surface, where dusty and quick illuviation occurred following deposition of sediment made of pedogenic aggregates, coarse lithogenic fraction and including abundant markers of anthropization (ceramic, bones). These features are typical of both massive deposits of pedosedimentary materials and anthropogenic deposits (Fedoroff, Courty, & Guo, 2010 ; Deák et al., 2017). Thus, geochemical and micromorphological data strongly support the previous hypothesis derived from field evidence*, i.e.* artificial and massive backfill of the basin probably accompanied by drainage works in the Late Iron Age or early Roman period (Mayoral et al., 2018), certainly to remediate the degraded situation of the wetland and extend the urban space. The post-Antiquity evolution of the basin is probably represented by SU1, however a lack of analytical and chronological data, and the interaction with present pedological activity prevent any detailed interpretation.

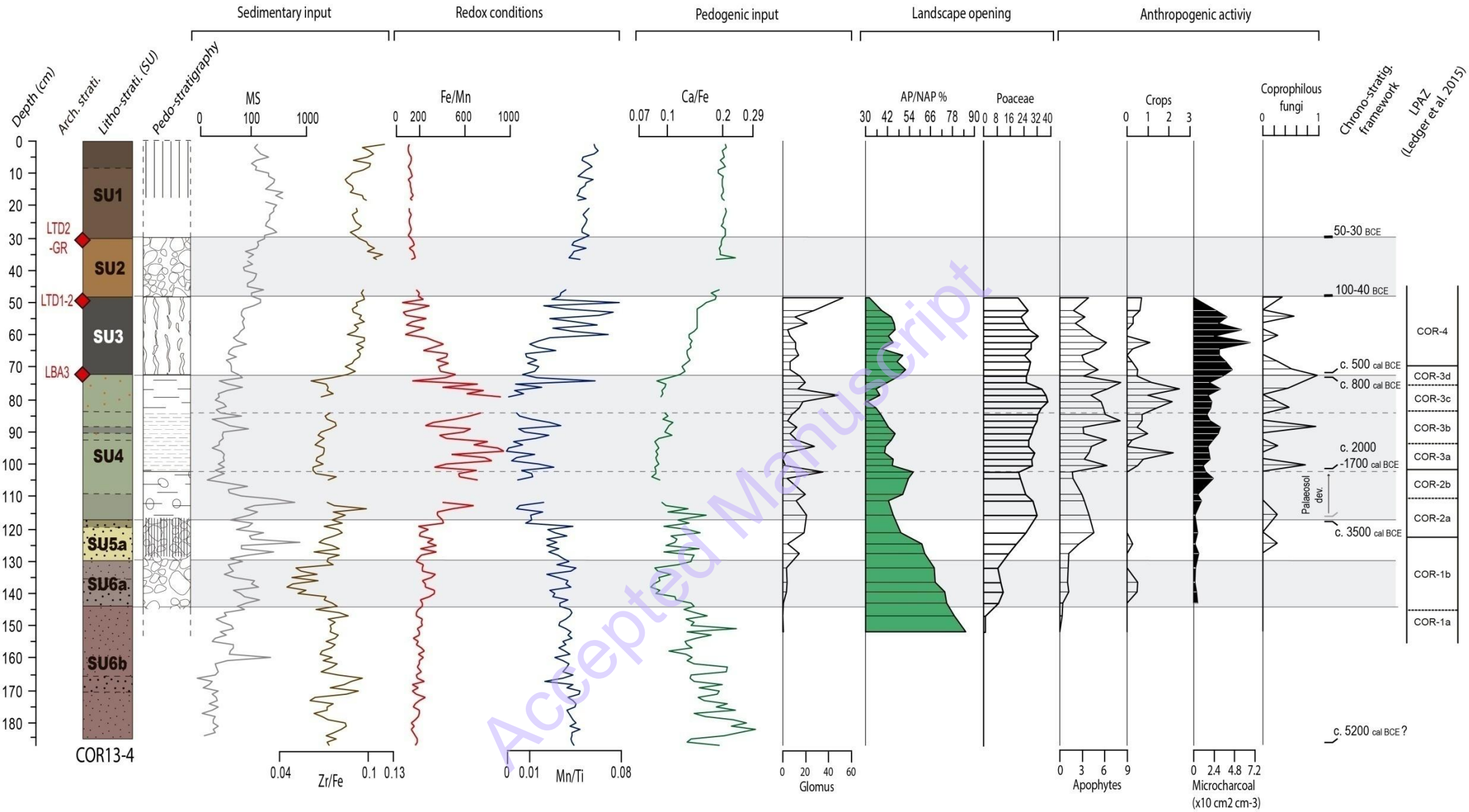

Figure 8. Synthetic multi-proxy diagram of COR13-4. Palynological, microcharcoal data and palynozones (LPAZ) are extracted from Ledger et al. (2015). Chronological landmarks are taken from chrono-stratigraphic framework, see Fig. 2. MS: Magnetic Susceptibility (SI.10^{-5}). AP: Arboreal Pollen. NAP: Non-Arboreal-Pollen. Pollen data are given as % of TLP (Total Land Pollen) - Lactuceae.

5-Conclusions

The general objective of this paper was to analyze long-term human-environment interactions at the Lac du Puy of Corent, a small wetland with a unique intra-urban setting within the protohistoric site of Corent. Building on previous studies, this paper employed a multi-proxy geoarchaeological approach of pedo-sedimentary archives of the Lac du Puy to address unresolved research questions, mainly concerning changing pedo-sedimentary processes and environmental conditions under human influence. New micromorphological, geochemical and sedimentological results were combined with existing palynological data within a refined chrono-stratigraphic framework. Micromorphological data in particular were used to disentangle the pedo-sedimentary processes, whose traces were superimposed in the complex pedo-sedimentary record. Geochemical proxies provided valuable and complementary data where micromorphology was equivocal, and pollen evidence was especially useful when discussing the impact of human activities on vegetation and soils. Data obtained in this, and previous studies were combined to provide a comprehensive understanding of complex human-environment interaction around the Lac du Puy since the Neolithic.

Here we have significantly refined previous interpretations, revealing anthropogenic impacts on vegetation, soil erosion and geomorphological processes probably began in the Early Neolithic, contemporary with the first traces of human activity on the plateau. These impacts gradually intensify until a shift at the end of the Middle Neolithic, associated with the development of a fortified settlement in the plateau.

In the Recent and Late Neolithic, anthropogenic impacts on soils tend to decrease and ultimately cease as human traces in the site become rare. Results of this study suggest that this abandonment is perhaps due to centuries of cumulated soils degradation. Our findings revealed a “hidden” phase of

1060 pedogenesis in the Lac du Puy basin between Recent Neolithic and the first centuries of the Early
1061 Bronze Age, with very low sedimentation rate. This phase of soil stability and vegetation recovery in
1062 the basin, and reduced erosion in the plateau, coincides with long-term abandonment of the
1063 occupation at Corent.

1064 During the Early Bronze Age, human agropastoral reappraisal of the plateau brings specific land use
1065 and management of the Lac du Puy. Micromorphology revealed that these new practices are
1066 certainly the anthropogenic catalyst of soil profile sealing and drainage degradation of the basin,
1067 which probably becomes a very stable wet grassland maintained by a feedback effect between
1068 agropastoral management, hydrosedimentary fluxes and pedogenic processes. From our results, two
1069 cycles of environmental impact can be distinguished in the later evolution of the basin during the
1070 Bronze Age. The first covers Early and Middle Bronze Age, and second the Late Bronze Age. Both start
1071 with reduced anthropogenic impacts characterized by pastoral and arable agriculture, and finish with
1072 drier and more detrital conditions. The clear association of the end of the later cycle with settlement
1073 expansion during Late Bronze Age 3 suggests that similar signal at the end of the Middle Bronze Age
1074 could have analogous causes. This implies an extended settlement during this period, which is not
1075 evident in existing archaeological data.

1076 The Iron Age is harder to interpret in the pedo-sedimentary record of the Lac du Puy. A major and
1077 permanent hydro-sedimentary change is noticeable in the basin, lasting despite the apparent demise
1078 of occupation during several centuries after abandonment of the Hallstatt site and associated storage
1079 pit battery. Geoarchaeological analysis shown that these “inherited” impacts are exacerbated by
1080 development of the *oppidum* in the late La Tène period, which presumably increased soil
1081 disturbance, erosion and runoff nourishing hydro-sedimentary inputs of the basin. Our study
1082 suggests that the Lac du Puy then becomes part of the sanitation/drainage system of the urban
1083 environment of the plateau and is recurrently flooded by hydro-sedimentary fluxes.
1084 Micromorphology confirmed that circa 50-30 BCE the area is backfilled probably in order to reclaim

this wasted space for urban area extension, however the function of this new space could not be determined. Later evolution of the basin after the Antiquity remains uncertain due to the lack of analytical and chronological data.

Results of this study draw a detailed multi-proxy picture of the complex evolution of socio-environmental interaction and human impacts on natural systems at Corent since the Early Neolithic. It contributes to refining our perceptions of the environmental impacts of prehistoric societies in Western Europe and highlights the crucial importance of keeping a long term perspective when dealing with past human-environment interactions.

6-Acknowledgements

This work was carried out as a part of the AYPONA project (dir. Y. Miras and F. Vautier), funded by the Conseil Régional d'Auvergne, the Service Régional d'Archéologie d'Auvergne, the Maison des Sciences de l'Homme de Clermont-Ferrand, and the University Lyon 2 (Projet BQR Lyon 2, dir. M. Poux and J-F. Berger). The authors are grateful to a number of people who contributed to this work. The archaeological team of Corent, and especially the LUERN association for providing logistic support, and Florian Couderc for valuable discussions. Pierre Boivin, Morgane Liard, Carlos Arteaga and Olivier Voldoire for their help with microscopy and micromorphological analyses. Anne-Lise Develle for her support in the analysis of XRF data. Adrien Barra provided assistance in laboratory work. Olivier Voldoire, Franck Vautier, Erwan Roussel, Aude Beauger, Emmanuelle Define, Gerard Vernet and Paul-Edgard Genet contributed in variable amounts to fieldwork. François-Xavier Simon and Bruno Depreux helped with geophysical and archaeological data respectively. Bertrand Dousteyssier contributed with aerial photography. We also owe our gratitude to the landowners Mme. Mioche and M. Rodriguez. Finally, we express sincere thanks to the anonymous reviewers for their remarks and critical reading of the manuscript.

7-Conflicts of interest

The authors declare no conflict of interest. The funding sponsors had no role in the design of the study; in the collection, analyses, or interpretation of data; in the writing of the manuscript, and in the decision to publish the results.

8-Appendix

SU	Depth (cm)	Munsell color	Description
1	0-30	10 YR 3/2	Dark brown clay loam, visible blocky to granular aggregation, basaltic granules, vegetal remains (topsoil)
2	30-49	10 YR 3/2	Dark brown clayey-silty loam, several basaltic granules, one amphorae sherd, some oxidation mottles.
3	49-72	10 YR 2,5/1	Very dark grey to black silty clay, rare oxidation mottles, basaltic sands and granules.
4	72-87	5 Y 4/2	Olive grey massive heavy clay, with abundant oxidation mottles in the top (above 83 cm), very rare sands and basaltic granules, one quartz gravel.
	87-89,5	5 Y 4/2 to 5 Y 3,5/2	Dark olive grey massive heavy clay, with some oxidation mottles, very rare sands and basaltic granules.
	89,5-92	5 Y 4/2	Olive grey massive heavy clay, with several oxidation mottles, very rare sands and basaltic granules.
	92-109	5 Y 4/2	Olive grey massive heavy clay, with some oxidation mottles, very rare sands and basaltic granules.
	109-117,5	5 Y 4/2 to 5 Y 3,5/2	Dark olive grey silty clay. Some oxidation mottles, rare sands and granules.
5A	117,5-119	10 YR 2,5/1 to 2,5 Y 3,5/2	Dark grey massive clayey silt, mottled aspect with fine sands and well-sorted small granules of scoria and basalt, weathered. Abundant dark grey and small clayey-silty granules, rounded.
	119-129	10 YR 3/1 to 2,5 Y 3,5/2	Dark grey massive clayey silt, mottled aspect with fine sands and well-sorted small granules of scoria and basalt, weathered. Dark grey or brown small clayey-silty granules, rounded.
6A	129-135	10 YR 4,5/1	Dark grey clayey silt, slightly mottled aspect with rare fine sands and small granules of scoria and basalt, weathered. Dark grey or brown small clayey-silty granules, rounded.
	135-144		Dark grey clayey silt, mottled aspect with fine sands and small granules of scoria and basalt, weathered. Dark grey or brown small clayey-silty granules, rounded.

6B	144-165	10 YR 4/1	Dark grey clayey silt, breccia-like mottled aspect with rare sands and dark reddish scoria and basaltic granules, weathered**.** Dark grey or brown small clayey-silty granules, rounded.
	165-170		Dark grey sandy silt, breccia-like mottled aspect with abundant fine to coarse sands and dark reddish scoria and basaltic granules, several fine to medium gravels, weathered**.**
	170-184		Dark grey clayey silt, breccia-like mottled aspect with some sands and dark reddish scoria, basaltic granules to fine/medium gravels, weathered**.** Dark grey small clayey granules, rounded.

Table 3. Litho-stratigraphic description of COR13-4

9-References

Adderley, W.P., Wilson, C.A., Simpson, I.A., Davidson, D.A., 2010. Anthropogenic Features, in: Interpretation of Micromorphological Features of Soils and Regoliths. Elsevier, pp. 569–588. https://doi.org/10.1016/B978-0-444-53156-8.00025-8

Anthony, J.W. (John W., 1990. Handbook of mineralogy. Mineral Data Pub.

Armit, I., Swindles, G.T., Becker, K., Plunkett, G., Blaauw, M., 2014. Rapid climate change did not cause population collapse at the end of the European Bronze Age. Proc. Natl. Acad. Sci. 111, 17045–17049. https://doi.org/10.1073/pnas.1408028111

Arnaud, F., Poulenard, J., Giguet-Covex, C., Wilhelm, B., Révillon, S., Jenny, J.-P., Revel, M., Enters, D., Bajard, M., Fouinat, L., Doyen, E., Simonneau, A., Pignol, C., Chapron, E., Vannière, B., Sabatier, P., 2016. Erosion under climate and human pressures : An alpine lake sediment perspective. Quat. Sci. Rev. 152, 1–18.

Baize, D., Girard, M.-C., 2008. Référentiel Pédologique. Quae.

Bajard, M., Poulenard, J., Sabatier, P., Develle, A.L., Giguet-Covex, C., Jacob, J., Crouzet, C., David, F., Pignol, C., Arnaud, F., 2017. Progressive and regressive soil evolution phases in the Anthropocene. Catena 150, 39–52. https://doi.org/10.1016/j.catena.2016.11.001

1137 Bajard, M., Sabatier, P., David, F., Develle, A.-L., Reyss, J.-L., Fanget, B., Malet, E., Arnaud, D.,
1138 Augustin, L., Crouzet, C., Poulenard, J., Arnaud, F., 2015. Erosion record in Lake La Thuile
1139 sediments (Prealps, France): Evidence of montane landscape dynamics throughout the
1140 Holocene. The Holocene 26, 350–364. https://doi.org/10.1177/0959683615609750

1141 Barker, G., 1985. Prehistoric Farming in Europe. Cambridge University Press.

1142 Bauer, A.M., Ellis, E.C., 2018. The Anthropocene Divide: Obscuring Understanding of Social-
1143 Environmental Change. Curr. Anthropol. 59, 000–000. https://doi.org/10.1086/697198

1144 Begon, J.C., Jamagne, M., 1973. Sur la genese de sols limoneux hydromorphes en France. Pseudogley
1145 Gley Genes. Use Hydromorphic Soils.

1146 Berger, Brochier, J.L., Vital, J., Delhon, C., Thiébault, S., 2007. Nouveau regard sur La dynamique des
1147 paysages et l'occupation humaine à L'Âge du Bronze en moyenne vallée du Rhône, in: Richard,
1148 H., Mordant, C., Magny, M. (Eds.), Environnements et Cultures à l'Age Du Bronze En Europe
1149 Occidentale. Editions du CTHS, Paris, p. 399.

1150 Berger, J.F., Delhon, C., Magnin, F., Bonté, S., Peyric, D., Thiébault, S., Guilbert, R., Beeching, A., 2016.
1151 A fluvial record of the mid-Holocene rapid climatic changes in the middle Rhone valley
1152 (Espeluche-Lalo, France) and of their impact on Late Mesolithic and Early Neolithic societies.
1153 Quat. Sci. Rev. 136, 66–84. https://doi.org/10.1016/j.quascirev.2015.11.019

1154 Bernigaud, N., Berger, J.-F., Bouby, L., Delhon, C., Latour-Argant, C., 2014. Ancient canals in the valley
1155 of Bourgoin-La Verpillière (France, Isère): morphological and geoarchaeological studies of
1156 irrigation systems from the Iron Age to the Early Middle Ages (8th century bc–6th century ad).
1157 Water Hist. 6, 73–93. https://doi.org/10.1007/s12685-013-0096-9

1158 Bini, M., Zanchetta, G., Persoiu, A., Cartier, R., Català, A., Cacho, I., Dean, J.R., Di Rita, F., Drysdale,
1159 R.N., Finnè, M., Isola, I., Jalali, B., Lirer, F., Magri, D., Masi, A., Marks, L., Mercuri, A.M., Peyron,

1160 O., Sadori, L., Sicre, M.-A., Welc, F., Zielhofer, C., Brisset, E., 2019. The 4.2 ka BP Event in the
1161 Mediterranean Region: an overview. Clim. Past 15, 555–577. https://doi.org/10.5194/cp-2018-
1162 147

1163 Birks, H.H., Birks, H.J.B., 2006. Multi-proxy studies in palaeolimnology. Veg. Hist. Archaeobot. 15,
1164 235–251. https://doi.org/10.1007/s00334-006-0066-6

1165 Blaauw, M., 2010. Methods and code for 'classical' age-modelling of radiocarbon sequences. Quat.
1166 Geochronol. 5, 512–518. https://doi.org/10.1016/J.QUAGEO.2010.01.002

1167 Blume, H.P., Brümmer, G.W., Fleige, H., Horn, R., Kandeler, E., Kögel-Knabner, I., Kretzschmar, R.,
1168 Stahr, K., Wilke, B.M., 2016. Scheffer/Schachtschabel Soil Science. Springer, Heidelberg; New
1169 York; Dordrecht; London. https://doi.org/10.1007/978-3-642-30942-7

1170 Bouiller, R., 1979. Minute de la carte Géologique de la France à 1:50000, feuille 717 (Veyre-Monton).

1171 Brammer, H., 1971. Coatings in seasonally flooded soils. Geoderma 6, 5–16.
1172 https://doi.org/10.1016/0016-7061(71)90047-4

1173 Brown, A., Toms, P., Carey, C., Rhodes, E., 2013. Geomorphology of the Anthropocene: Time-
1174 transgressive discontinuities of human-induced alluviation. Anthropocene 1, 3–13.
1175 https://doi.org/10.1016/j.ancene.2013.06.002

1176 Bullock, P., Fedoroff, N., Jongerius, A., Stoops, G., Tursina, T., Babel, U., 1985. Handbook for soil thin
1177 section description. WAINE Research publications, Wolverhampton.

1178 Burga, C.A., Perret, R., Zoller, H., 2001. Swiss localities of early recognized Holocene climate
1179 oscillations: Characterization and significance. Vierteljahrsschrift der Naturforschenden
1180 Gesellschaft Zuerich 146, 65–74.

1181 Butzer, K., 2015. Anthropocene as an evolving paradigm. Holocene 25, 1539–1541.
1182 https://doi.org/10.1177/0959683615594471

1183 Butzer, K.W., 2011. Geoarchaeology, Climate Change and Sustainability: A Mediterranean
1184 perspective. Geol. Soc. Am. Pap. 476, 15. https://doi.org/10.1130/2011.2476(01).

1185 Butzer, K.W., 2008. Challenges for a cross-disciplinary geoarchaeology: The intersection between
1186 environmental history and geomorphology. Geomorphology 101, 402–411.
1187 https://doi.org/10.1016/j.geomorph.2008.07.007

1188 Buurman, P., Jongmans, a. G., PiPujol, M.D., 1998. Clay illuviation and mechanical clay infiltration —
1189 Is there a difference? Quat. Int. 51–52, 66–69. https://doi.org/10.1016/S1040-6182(98)90225-7

1190 Carozza, L., Berger, J., Burens, A., Marcigny, C., 2015. Society and environment in Southern France
1191 from the 3rd millenium BC to the beginning of the 2d millenium BC a tipping point?, in: 2200 BC
1192 – Ein Klimasturz Als Ursache Für Den Zerfall Der Alten Welt ? 2200 BC – A Climatic Breakdown
1193 as a Cause for the Collapse of the Old World ? pp. 833–844.

1194 Carozza, L., Marcigny, C., Burens Carozza, A., Ghesquiere, E., 2007. Les travaux et les jours : la lente
1195 transformation des sociétés paysannes de l'âge du Bronze en France métropolitaine 42–56.

1196 Carter, S., Davidson, D., 1998. An Evaluation of the Contribution of Soil Micromorphology to the
1197 Study of Ancient Arable Agriculure. Geoarchaeology An Int. J. 13, 549–564.
1198 https://doi.org/10.1002/(SICI)1520-6548(199808)13:6<549::AID-GEA2>3.0.CO;2-Z

1199 Cartier, R., Sylvestre, F., Paillès, C., Sonzogni, C., Couapel, M., Alexandre, A., Mazur, J.C., Brisset, E.,
1200 Miramont, C., Guiter, F., 2019. Diatom-oxygen isotope record from high-altitude Lake Petit
1201 (2200 m a.s.l.) in the Mediterranean Alps: Shedding light on a climatic pulse at 4.2 ka. Clim. Past
1202 15, 253–263. https://doi.org/10.5194/cp-15-253-2019

1203 Corella, J.P., Benito, G., Rodriguez-Lloveras, X., Brauer, A., Valero-Garcés, B.L., 2014. Annually-
1204 resolved lake record of extreme hydro-meteorological events since AD 1347 in NE Iberian
1205 Peninsula. Quat. Sci. Rev. 93, 77–90. https://doi.org/10.1016/j.quascirev.2014.03.020

1206 Corella, J.P., Brauer, A., Mangili, C., Rull, V., Vegas-Vilarrúbia, T., Morellón, M., Valero-Garcés, B.L.,
1207 2012. The 1.5-ka varved record of Lake Montcortès (southern Pyrenees, NE Spain). Quat. Res.
1208 78, 323–332. https://doi.org/10.1016/J.YQRES.2012.06.002

1209 Courty, M.A., Fedoroff, N., 2002. Micromorphologie des sols et sédiments archéologiques. Géologie
1210 la Préhistoire 511–554.

1211 Cremaschi, M., 2014. When did the Anthropocene begin? A geoarchaeological approach to
1212 deciphering the consequences of human activity in pre-protohistoric times: Selected cases from
1213 the Po Plain (northern Italy). Rend. Lincei 25, 101–112. https://doi.org/10.1007/s12210-013-
1214 0266-9

1215 Cremaschi, M., Mercuri, A.M., Torri, P., Florenzano, A., Pizzi, C., Marchesini, M., Zerboni, A., 2016.
1216 Climate change versus land management in the Po Plain (Northern Italy) during the Bronze Age:
1217 New insights from the VP/VG sequence of the Terramara Santa Rosa di Poviglio. Quat. Sci. Rev.
1218 136, 153–172. https://doi.org/10.1016/j.quascirev.2015.08.011

1219 Crutzen, P.J., Stoermer, E.F., 2000. The "Anthropocene." Glob. Chang. Newsl. 41, 17–18.

1220 Cuven, S., Francus, P., Lamoureux, S., 2011. Mid to Late Holocene hydroclimatic and geochemical
1221 records from the varved sediments of East Lake, Cape Bounty, Canadian High Arctic. Quat. Sci.
1222 Rev. 30, 2651–2665. https://doi.org/10.1016/J.QUASCIREV.2011.05.019

1223 Dalan, R.A., 2017. Susceptibility, in: Gilbert, A.S. (Ed.), Encyclopedia of Geoarchaeology. Springer
1224 Netherlands, Dordrecht, pp. 939–943. https://doi.org/10.1007/978-1-4020-4409-0_170

1225 Danielisova, A., Hajnalova, M., 2014. OPPIDA AND AGRICULTURAL PRODUCTION – STATE OF THE ART
1226 AND PROSPECTS . CASE STUDY FROM STARÉ HRADISKO OPPIDUM (CZECH REPUBLIC), in:
1227 Hornung, S. (Ed.), Produktion - Distribution - Ökonomie Siedlungs- Und Wirtschaftsmuster Der
1228 Latènezeit. Habelt Verlag, pp. 407–428.

1229 Daugas, J.P., 1972. Une fosse à inhumations néolithique à Corent (Puy-de-Dôme). Congrès
1230 Préhistorique Fr. XIXe Sess. Auvergne 1969 183–189.

1231 Davidson, D.A., Carter, S.P., 1998. Micromorphological evidence of past agricultural practices in
1232 cultivated soils: the impact of a traditional agricultural system on soils in Papa Stour, Shetland.
1233 J. Archaeol. Sci. 25, 827–838. https://doi.org/10.1006/jasc.1997.0225

1234 Davies, S.J., Lamb, H.F., Roberts, S.J., 2015. Micro-XRF Core Scanning in Palaeolimnology: Recent
1235 Developments, in: Croudace, I.W., Rothwell, R.G. (Eds.), Micro-XRF Studies of Sediment Cores:
1236 Applications of a Non-Destructive Tool for the Environmental Sciences. Springer Netherlands,
1237 Dordrecht, pp. 189–226. https://doi.org/10.1007/978-94-017-9849-5_7

1238 Deák, J., Gebhardt, A., Lewis, H., Usai, M.R., Lee, H., 2017. Soils Disturbed by Vegetation Clearance
1239 and Tillage, in: Archaeological Soil and Sediment Micromorphology. John Wiley & Sons, Ltd,
1240 Chichester, UK, pp. 231–264. https://doi.org/10.1002/9781118941065.ch28

1241 Dearing, J., 1999. Magnetic susceptibility. Environ. Magn. A Pract. Guid. 6, 35–62.

1242 Dearing, J.A., 2006. Climate-human-environment interactions: Resolving our past. Clim. Past 2, 187–
1243 203. https://doi.org/10.5194/cp-2-187-2006

1244 Delvigne, J., 1998. Atlas of Micromorphology of Mineral Alteration and Weathering, The canadian
1245 Mineralogist.

1246 Dubois, N., Saulnier-Talbot, É., Mills, K., Gell, P., Battarbee, R., Bennion, H., Chawchai, S., Dong, X.,
1247 Francus, P., Flower, R., Gomes, D.F., Gregory-Eaves, I., Humane, S., Kattel, G., Jenny, J., Langdon,
1248 P., Massaferro, J., McGowan, S., Mikomägi, A., Ngoc, N.T.M., Ratnayake, A.S., Reid, M., Rose, N.,
1249 Saros, J., Schillereff, D., Tolotti, M., Valero-Garcés, B., 2018. First human impacts and responses
1250 of aquatic systems: A review of palaeolimnological records from around the world. Anthr. Rev.
1251 205301961774036. https://doi.org/10.1177/2053019617740365

1252 Fedoroff, N., Courty, M.-A., 2002. Paléosols et sols reliques. Miskovsky JC Géologie la préhistoire,
1253 Assoc. pour l'étude l'environnement géologique la préhistoire, Paris 277–316.

1254 Fedoroff, N., Courty, M.-A., Guo, Z., 2010. Palaeosoils and Relict Soils, in: Interpretation of
1255 Micromorphological Features of Soils and Regoliths. Elsevier, pp. 623–662.
1256 https://doi.org/10.1016/B978-0-444-53156-8.00027-1

1257 Fernández-Götz, M., 2018. Urbanization in Iron Age Europe: Trajectories, Patterns, and Social
1258 Dynamics. J. Archaeol. Res. 26, 117–162. https://doi.org/10.1007/s10814-017-9107-1

1259 Foley, S.F., Gronenborn, D., Andreae, M.O., Kadereit, J.W., Esper, J., Scholz, D., Pöschl, U., Jacob, D.E.,
1260 Schöne, B.R., Schreg, R., Vött, A., Jordan, D., Lelieveld, J., Weller, C.G., Alt, K.W., Gaudzinski-
1261 Windheuser, S., Bruhn, K.C., Tost, H., Sirocko, F., Crutzen, P.J., 2013. The Palaeoanthropocene -
1262 The beginnings of anthropogenic environmental change. Anthropocene 3, 83–88.
1263 https://doi.org/10.1016/j.ancene.2013.11.002

1264 García-Alix, A., Jimenez-Espejo, F.J., Lozano, J.A., Jiménez-Moreno, G., Martinez-Ruiz, F., García
1265 Sanjuán, L., Aranda Jiménez, G., García Alfonso, E., Ruiz-Puertas, G., Anderson, R.S., 2013.
1266 Anthropogenic impact and lead pollution throughout the Holocene in Southern Iberia. Sci. Total
1267 Environ. 449, 451–460. https://doi.org/10.1016/j.scitotenv.2013.01.081

1268 Gauthier, E., Richard, H., Magny, M., Peyron, O., Arnaud, F., Jacob, J., Marguet, A., Billaud, Y., 2008.
1269 Le lac du Bourget (Savoie , France) à l ' Age du Bronze : végétation , impacts anthropiques et
1270 climat, in: Richard, H., Garcia, D. (Eds.), Le Peuplement de l'arc Alpin. Paris, pp. 107–121.

1271 Greffier, G., Restituito, J., Héraud, H., 1980. Aspects géomorphologiques et stabilité des versants au
1272 sud de Clermont-Ferrand. Bull. liaison du Lab. des Ponts Chaussées 107, 17–26.

1273 Grimm, E.C., Maher, L.J., Nelson, D.M., 2009. The magnitude of error in conventional bulk-sediment
1274 radiocarbon dates from central North America. Quat. Res. 72, 301–308.

https://doi.org/10.1016/j.yqres.2009.05.006

Guichard, V., 1991. Puy de Corent (Puy-de-Dôme) rapport de prospection et sondages.

Guillemoteau, J., Simon, F.-X., Lück, E., Tronicke, J., 2016. 1D sequential inversion of portable multi-configuration electromagnetic induction data. Near Surf. Geophys. 411–420. https://doi.org/10.3997/1873-0604.

Gutiérrez-Castorena, M. del C., Effland, W.R., 2010. Pedogenic and Biogenic Siliceous Features, in: Interpretation of Micromorphological Features of Soils and Regoliths. Elsevier, pp. 471–496. https://doi.org/10.1016/B978-0-444-53156-8.00021-0

Haas, M., Baumann, F., Castella, D., Haghipour, N., Reusch, A., Strasser, M., Eglinton, T.I., Dubois, N., 2019. Roman-driven cultural eutrophication of Lake Murten, Switzerland. Earth Planet. Sci. Lett. 505, 110–117. https://doi.org/10.1016/j.epsl.2018.10.027

Haberzettl, T., Corbella, H., Fey, M., Janssen, S., Lücke, A., Mayr, C., Ohlendorf, C., Schäbitz, F., Schleser, G.H., Wille, M., Wulf, S., Zolitschka, B., 2007. Lateglacial and Holocene wet—dry cycles in southern Patagonia: chronology, sedimentology and geochemistry of a lacustrine record from Laguna Potrok Aike, Argentina. The Holocene 17, 297–310. https://doi.org/10.1177/0959683607076437

Hausmann, J., Zielhofer, C., Werther, L., Berg-Hobohm, S., Dietrich, P., Heymann, R., Werban, U., 2018. Direct push sensing in wetland (geo)archaeology: High-resolution reconstruction of buried canal structures (Fossa Carolina, Germany). Quat. Int. 473, 21–36. https://doi.org/10.1016/j.quaint.2017.02.008

Houben, P., Wunderlich, J., Schrott, L., 2009. Climate and long-term human impact on sediment fluxes in watershed systems. Geomorphology 108, 1–7. https://doi.org/10.1016/j.geomorph.2008.08.018

1298 Huisman, D.J., Braadbaart, F., van Wijk, I.M., van Os, B.J.H., 2012. Ashes to ashes, charcoal to dust:
1299 Micromorphological evidence for ash-induced disintegration of charcoal in Early Neolithic (LBK)
1300 soil features in Elsloo (The Netherlands). J. Archaeol. Sci. 39, 994–1004.
1301 https://doi.org/10.1016/j.jas.2011.11.019

1302 Jamagne, M., 1978. Les processus pédogénétiques dans une séquence évolutive progressive sur
1303 formations limoneuses loessiques en zone tempérée froide et humide. Comptes Rendus
1304 l'Académie des Sci. 286, 25–27.

1305 Jongerius, A., 1970. Some morphological aspects of regrouping phenomena in dutch soils. Geoderma
1306 4.

1307 Jongmans, a. G., Feijtel, T.C.J., Miedema, R., van Breemen, N., Veldkamp, a., 1991. Soil formation in
1308 a Quaternary terrace sequence of the Allier, Limagne, France. Macro- and micromorphology,
1309 particle size distribution, chemistry. Geoderma 49, 215–239. https://doi.org/10.1016/0016-
1310 7061(91)90077-7

1311 Jongmans, A.., Van Doesburgl, J.D.., Van Breement, N., 1990. Micromorphology and mineralogy of
1312 weathering and neoformation phenomena in a quaternary terrace sequence of the Allier,
1313 Limagne, France, in: Geochemitry of the Earths Surface and of Mineral Formation 2nd
1314 International Symposium. Aix en Provence, France, pp. 83–85.

1315 Kabata-Pendias, A., Pendias, H., 2001. Trace elements in soils and plants, New York.
1316 https://doi.org/10.1201/b10158-25

1317 Kaniewski, D., Van Campo, E., Morhange, C., Guiot, J., Zviely, D., Shaked, I., Otto, T., Artzy, M., 2013.
1318 Early urban impact on Mediterranean coastal environments. Sci. Rep. 3, 1–5.
1319 https://doi.org/10.1038/srep03540

1320 Kooistra, M.J., Pulleman, M.M., 2010. Features Related to Faunal Activity, in: Interpretation of

1321 Micromorphological Features of Soils and Regoliths. Elsevier, pp. 397–418.
1322 https://doi.org/10.1016/B978-0-444-53156-8.00018-0

1323 Kovda, I., Mermut, A.R., 2010. Vertic Features, in: Interpretation of Micromorphological Features of
1324 Soils and Regoliths. Elsevier, pp. 109–127. https://doi.org/10.1016/B978-0-444-53156-8.00007-
1325 6

1326 Kühn, P., Aguilar, J., Miedema, R., 2010. Textural Pedofeatures and Related Horizons, in:
1327 Interpretation of Micromorphological Features of Soils and Regoliths. Elsevier, pp. 217–250.
1328 https://doi.org/10.1016/B978-0-444-53156-8.00011-8

1329 Kylander, M.E., Ampel, L., Wohlfarth, B., Veres, D., 2011. High-resolution X-ray fluorescence core
1330 scanning analysis of Les Echets (France) sedimentary sequence: new insights from chemical
1331 proxies. J. Quat. Sci. 26, 109–117. https://doi.org/10.1002/jqs.1438

1332 Ledger, P.M., Edwards, K.J., Schofield, J.E., 2017. Competing hypotheses, ordination and pollen
1333 preservation: Landscape impacts of Norse landnám in southern Greenland. Rev. Palaeobot.
1334 Palynol. 236, 1–11. https://doi.org/10.1016/j.revpalbo.2016.10.007

1335 Ledger, Paul M., Edwards, K.J., Schofield, J.E., 2015. Taphonomy or signal sensitivity in
1336 palaeoecological investigations of Norse landnam in Vatnahverfi, southern Greenland? Boreas
1337 44, 197–215. https://doi.org/10.1111/bor.12089

1338 Ledger, Paul M, Miras, Y., Poux, M., Milcent, P.Y., 2015. The palaeoenvironmental impact of
1339 prehistoric settlement and proto-historic urbanism: tracing the emergence of the oppidum of
1340 corent, auvergne, france. PLoS One 10, e0121517.
1341 https://doi.org/10.1371/journal.pone.0121517

1342 Legrand, P., Bartoli, F., Curt, T., 2007. Spécificités des sols volcaniques du Massif Central: bénéfices et
1343 contraintes pour la gestion forestière. Rev. For. Française 59.

1344 Lespez, L., Carozza, L., Berger, J., Kuzucuoğlu, C., Ghilardi, M., Carozza, J., Vannière, B., 2016. Rapid
1345 climatic change and social transformations Uncertainties, adaptability and resilience, in: The
1346 Mediterranean Region under Climate Change-A Scientific Update. AllEnvi, p. 738.

1347 Lewis, S.L., Maslin, M.A., 2015. Defining the Anthropocene. Nature 519, 171–180.
1348 https://doi.org/10.1038/nature14258

1349 Lindbo, D.L., Stolt, M.H., Vepraskas, M.J., 2010. Redoximorphic Features, in: Interpretation of
1350 Micromorphological Features of Soils and Regoliths. Elsevier, pp. 129–147.
1351 https://doi.org/10.1016/B978-0-444-53156-8.00008-8

1352 Loaiza, J.C., Stoops, G., Poch, R.M., Casamijtana, M., 2015. Manual de micromorfología de suelos y
1353 técnicas complementarias. Fondo Editor. Pascual Bravo 348.

1354 Macaire, J.J., Fourmont, A., Argant, J., Bréhéret, J.G., Hinschberger, F., Trément, F., 2010.
1355 Quantitative analysis of climate versus human impact on sediment yield since the Lateglacial:
1356 The Sarlève palaeolake catchment (France). The Holocene 20, 497–516.
1357 https://doi.org/10.1177/0959683609355181

1358 MacKenzie, W.S., Donaldson, C.H., Guilford, C., 1982. Atlas of Igneous Rocks and Their Textures.
1359 ELBS.

1360 Macphail, R.I., 1998. A reply to Carter and Davidson's "an evaluation of the contribution of soil
1361 micromorphology to the study of ancient arable agriculture. Geoarchaeology An Int. J. 13, 549–
1362 564. https://doi.org/10.1002/(SICI)1520-6548(199808)13:6<549::AID-GEA2>3.0.CO;2-Z

1363 Macphail, R.I., Courty, M.A., Gebhardt, A., 1990. Soil micromorphological evidence of early
1364 agriculture in north-west Europe. World Archaeol. 22, 53–69.
1365 https://doi.org/10.1080/00438243.1990.9980129

1366 Macphail, R.I., Goldberg, P., 2018. Applied Soils and Micromorphology in Archaeology. Cambridge

1367 Manuals in Archaeology-Cambridge University Press, Cambridge.

1368 Magny, M., Leuzinger, U., Bortenschlager, S., Haas, J.N., 2006. Tripartite climate reversal in Central
1369 Europe 5600-5300 years ago. Quat. Res. 65, 3–19. https://doi.org/10.1016/j.yqres.2005.06.009

1370 Magny, M., Vannière, B., Zanchetta, G., Fouache, E., Touchais, G., Petrika, L., Coussot, C., Walter-
1371 Simonnet, A.V., Arnaud, F., 2009. Possible complexity of the climatic event around 4300-3800
1372 cal. BP in the central and western Mediterranean. Holocene 19, 823–833.
1373 https://doi.org/10.1177/0959683609337360

1374 Magny, Peyron, O., Gauthier, E., Rouèche, Y., Bordon, A., Billaud, Y., Chapron, E., Marguet, A.,
1375 Pétrequin, P., Vannière, B., 2009. Quantitative reconstruction of climatic variations during the
1376 Bronze and early Iron ages based on pollen and lake-level data in the NW Alps, France. Quat.
1377 Int. 200, 102–110. https://doi.org/10.1016/j.quaint.2008.03.011

1378 Martín-Puertas, C., Valero-Garcés, B.L., Brauer, A., Mata, M.P., Delgado-Huertas, A., Dulski, P., 2009.
1379 The Iberian-Roman Humid Period (2600-1600 cal yr BP) in the Zoñar Lake varve record
1380 (Andalucía, southern Spain). Quat. Res. 71, 108–120.
1381 https://doi.org/10.1016/j.yqres.2008.10.004

1382 Martínez Cortizas, A., López-Merino, L., Bindler, R., Mighall, T., Kylander, M.E., 2016. Early
1383 atmospheric metal pollution provides evidence for Chalcolithic/Bronze Age mining and
1384 metallurgy in Southwestern Europe. Sci. Total Environ. 545–546, 398–406.
1385 https://doi.org/10.1016/j.scitotenv.2015.12.078

1386 Mayewski, P.A., Rohling, E.E., Stager, J.C., Karlén, W., Maasch, K.A., Meeker, L.D., Meyerson, E.A.,
1387 Gasse, F., van Kreveld, S., Holmgren, K., Lee-Thorp, J., Rosqvist, G., Rack, F., Staubwasser, M.,
1388 Schneider, R.R., Steig, E.J., 2004. Holocene climate variability. Quat. Res. 62, 243–255.
1389 https://doi.org/10.1016/j.yqres.2004.07.001

1390 Mayfield, C.I., Williams, S.T., Ruddick, S.M., Hatfield, H.L., 1972. Studies on the ecology of
1391 actinomycetes in soil IV. Observations on the form and growth of Streptomycetes in soil. Soil
1392 Biol. Biochem. 47, 79–91. https://doi.org/10.1016/0038-0717(70)90029-5

1393 Mayoral, A., Depreux, B., 2017. Lac du Puy de Corent-Opération 2015: Sondages Géoarchéologiques-
1394 Rapport de prospection thématique.

1395 Mayoral, A., Peiry, J.-L., Berger, J., Ledger, P.M., Depreux, B., Simon, F.X., Milcent, P.-Y., Poux, M.,
1396 Vautier, F., Miras, Y., 2018. Geoarchaeology and chronostratigraphy of the Lac du Puy intra-
1397 urban protohistoric wetland, Corent, France. Geoarchaeology.

1398 Mayoral, A., Peiry, J.-L., Berger, J., Vautier, F., Miras, Y., 2017. LA APORTACIÓN DEL LIDAR A LA
1399 CARTOGRAFÍA GEOMORFOLÓGICA DE DETALLE Y AL ANÁLISIS DE POTENCIAL
1400 GEOARQUEOLÓGICO: EL EJEMPLO DEL PUY DE CORENT (AUVERNIA, FRANCIA)., in: Actas Del
1401 XXV Congreso de La Asociación de Geógrafos Españoles. UAM Ediciones, Madrid, p. 2762.

1402 Mielke, J.E., 1979. Composition of the Earth's crust and distribution of the elements. Rev. Res. Mod.
1403 Probl. geochemistry 13–37.

1404 Milcent, P.-Y., Chassan, N., Mader, S., Saint-Sever, G., Tramon, A., 2014a. Les occupations de l'âge du
1405 Bronze du plateau de Corent (Auvergne, Puy-de-Dôme) : résultats des campagnes de fouille
1406 2010-2013. Bull. APRAB 12, 89–94.

1407 Milcent, P.-Y., Poux, M., Mader, S., Torres, M., Tramon, A., 2014b. Une agglomération de hauteur
1408 autour de 600 a.C. en Gaule centrale : Corent (Auvergne). Transalpinare 181–204.

1409 Miras, Y., Laggoun-Defarge, F., Guenet, P., Richard, H., 2004. Multi-disciplinary approach to changes
1410 in agro-pastoral activities since the Sub-Boreal in the surroundings of the "Narse d'Espinasse"
1411 (Puy de Dome, French Massif Central). Veg. Hist. Archaeobot. 13, 91–103.
1412 https://doi.org/10.1007/s00334-004-0033-z

Miras, Y., Mariani, M., Couderc, F., Lavrieux, M., Ledger, P.M., 2018. Addressing the complexity of the paleoenvironmental impact of Prehistoric settlement and Protohistoric urbanism in the Auvergne Mountains (Massif Central, France), in: IEMA VOLUME-ARCHAEOLOGY OF MOUNTAIN LANDSCAPES: INTERDISCIPLINARY RESEARCH STRATEGIES OF AGRO-PASTORALISM IN UPLAND REGIONS.

Nehlig, P., Boivin, P., De Goër, A., Mergoil, J., Sustrac, G., Thiéblemont, D., 2003. Les volcans du Massif central. Géologues (sp. issue) 1–41.

Néraudeau, D., Martin, S. Saint, Batten, D.J., Colin, J.P., Daviero-Gomez, V., Girard, V., Gomez, B., Nohra, Y.A., Polette, F., Platel, J.P., Martin, J.P.S., Vullo, R., 2016. Palaeontology of the upper Turonian paralic deposits of the Sainte-Mondane formation, Aquitaine basin, France. Geol. Acta 14, 53–69. https://doi.org/10.1344/GeologicaActa2016.14.1.5

Néraudeau, D., Perrichot, V., Batten, D.J., Boura, A., Girard, V., Jeanneau, L., Nohra, Y.A., Polette, F., Martin, S. Saint, Saint Martin, J.P., Thomas, R., 2017. Upper Cretaceous amber from Vendée, north-western France: Age dating and geological, chemical, and palaeontological characteristics. Cretac. Res. 70, 77–95. https://doi.org/10.1016/j.cretres.2016.10.001

Nicosia, C., Stoops, G., 2017. Archaeological Soil and Sediment Micromorphology. Wiley Blackwell.

Notebaert, B., Berger, J., 2014. Quantifying the anthropogenic forcing on soil erosion during the Iron Age and Roman Period in southeastern France. Anthropocene 8, 59–69. https://doi.org/10.1016/j.ancene.2015.05.004

Notebaert, B., Broothaerts, N., Verstraeten, G., 2018. Evidence of anthropogenic tipping points in fluvial dynamics in Europe. Glob. Planet. Change 164. https://doi.org/10.1016/j.gloplacha.2018.02.008

Osman, K.T., 2013. Soils: Principles, properties and management. Springer Netherlands, Dordrecht,

1436 Heidelberg, New York, London. https://doi.org/10.1007/978-94-007-5663-2

1437 Pavelka, J., Smetanova, A., Rejman, J., Kovacik, P., 2017. AN INTERDISCIPLINARY TILLAGE EROSION
1438 EXPERIMENT : ESTABLISHING A NEW FIELD IN GRASSLANDS WITH RECONSTRUCTED ARD
1439 PLOUGH OF THE BRONZE AGE - IRON AGE. Cuad. Investig. Geográfica 43, 101–118.

1440 Peña-Monné, J.L., 2018. Geoarqueología aplicada a la reconstrucción paleoambiental : La evolución
1441 del Holoceno superior en el NE de España. Boletín Geológico y Min. 129, 285–303.
1442 https://doi.org/10.21701/bolgeomin.129.1.011

1443 Pétrequin, P., Weller, O., 2007. xve siècle av. J.-C. : la reprise de la croissance démographique dans le
1444 Jura, in: Environnements et Cultures à l'Âge Du Bronze En Europe Occidentale, Actes Du 129e
1445 Congrès National Des Sociétés Historiques et Scientifiques (Besançon, 2004). CTHS (Documents
1446 préhistoriques, 21), Paris, pp. 197–210.

1447 Poux, M., 2012. Corent, Voyage au coeur d'une ville gauloise. Editions Errance, Paris.

1448 Poux, M., Milcent, P.-Y., Pranyies, A., Lauranson, R., Dubreu, N., Chorin, A., Evrard, M., Hemard, C.,
1449 Mader, S., Philibeaux, R., Tramon, A., Valfort, P., Duchamp, H., Demierre, M., Crausaz, A., Gruel,
1450 K., 2016. Corent, Rapport de fouille programmée 2015.

1451 Poux, M., Milcent, P.-Y., Pranyies, A., Mader, S., Laurenson, R., Courtot, A., Dubreu, N., Brossard, C.,
1452 Chorin, A., Evrard, M., Freycon, F., Garcia, M., Hemard, C., Millet, M., Roussel, C., Philibeaux, R.,
1453 Sivignon, R., Sonn, M., Tramon, A., Couderc, F., Lavail, C., Valfort, P., Demierre, M., Crausaz, A.,
1454 Duchamp, H., Gruel, K., Meiraud, A., 2018. Corent, Fouille pluriannuelle 2014-2016, Rapport
1455 Final d'Opération.

1456 Reimer, P.J., Bard, E., Bayliss, A., Beck, J.W., Blackwell, P.G., Bronk Ramsey, C., Buck, C.E., Cheng, H.,
1457 Edwards, R.L., Friedrich, M., Grootes, P.M., Guilderson, T.P., Haflidason, H., Hajdas, I., Hatté, C.,
1458 Heaton, T.J., Hoffmann, D.L., Hogg, A.G., Hughen, K.A., Kaiser, K.F., Kromer, B., Manning, S.W.,

1459 Niu, M., Reimer, R.W., Richards, D.A., Scott, E.M., Southon, J.R., Staff, R.A., Turney, C.S.M., van
1460 der Plicht, J., 2013. IntCal13 and Marine13 Radiocarbon Age Calibration Curves 0–50,000 Years
1461 cal BP. Radiocarbon 55, 1869–1887. https://doi.org/10.2458/azu_js_rc.55.16947

1462 Retallack, G.J., 2001. Soils of the past. An introduction to paleopedology. Blackwell Science.

1463 Rey, F., 2005. Efficacité des ouvrages de génie biologique pour le piégeage des sédiments dans des
1464 ravines incisées dans des marnes (Alpes du Sud, France). Géomorphologie Reli. Process.
1465 Environ. 11, 21–30.

1466 Ringrose-Voase, A.J., Humphreys, G.S., 1994. Soil Micromorphology: studies in management and
1467 genesis. Elsevier, Amsterdam.

1468 Roberts, C.N., Woodbridge, J., Palmisano, A., Bevan, A., Fyfe, R., Shennan, S., 2019. Mediterranean
1469 landscape change during the Holocene: Synthesis, comparison and regional trends in
1470 population, land cover and climate. Holocene 29, 923–937.
1471 https://doi.org/10.1177/0959683619826697

1472 Rösch, M., 2013. Land use and food production in Central Europe from the Neolithic to the Medieval
1473 period: change of landscape, soils and agricultural systems according to archaeobotanical data.
1474 Econ. Archaeol. from Struct. to Perform. Eur. Archaeol. 109–127.

1475 Rösch, M., 1998. The history of crops and crop weeds in south-western Germany from the Neolithic
1476 period to modern times, as shown by archaeobotanical evidence. Veg. Hist. Archaeobot. 7,
1477 109–125. https://doi.org/10.1007/BF01373928

1478 Ruddiman, W., 2017. Geographic evidence of the early anthropogenic hypothesis. Anthropocene 20,
1479 4–14. https://doi.org/10.1016/j.ancene.2017.11.003

1480 Ruddiman, W.F., Ellis, E.C., Kaplan, J.O., Fuller, D.Q., 2015. Defining the epoch we live in. Is a formally
1481 designated “Anthropocene” a good idea? Science (80-.). 348, 38–39.

https://doi.org/10.1126/science.aaa7297

Sabatier, P., Dezileau, L., Briqueu, L., Colin, C., Siani, G., 2010. Clay minerals and geochemistry record from northwest Mediterranean coastal lagoon sequence: Implications for paleostorm reconstruction. Sediment. Geol. 228, 205–217. https://doi.org/10.1016/J.SEDGEO.2010.04.012

Salminen, R., Batista, M.J., Bidovec, M., Demetriades, A., De Vivo, B., De Vos, W., 2005. FOREGS Geochemical Atlas of Europe, Part I* Background Information, Methodology, and Maps. Geol. Surv. Finland, Espoo.

Sedov, S., Stoops, G., Shoba, S., 2010. Regoliths and Soils on Volcanic Ash, in: Interpretation of Micromorphological Features of Soils and Regoliths. Elsevier, pp. 275–303. https://doi.org/10.1016/B978-0-444-53156-8.00013-1

Siklosy, Z., Demeny, A., Vennemann, T.W., Kramers, J., Lauritzen, S.E., 2007. Middle bronze age climate change recorded in a Hungarian stalagmite : triggering by volcanic activity ? Holocene 9, 2–3.

Slager, S., van de Wetering, H.T.J., 1977. Soil formation in archaeological pits and adjacent loess soils in Southern Germany. J. Archaeol. Sci. 4, 259–267. https://doi.org/10.1016/0305-4403(77)90093-0

Stoops, 2003. Guidelines for Analysis and Description of soil and Regolith Thin Sections. Soil Science Society of America, Madison, Wisconsin.

Stoops, G., Marcelino, V., Mees, F., 2010a. Interpretation of Micromorphological features of soils and regoliths. Elsevier, Amsterdam.

Stoops, G., Marcelino, V., Mees, F., 2010b. Micromorphological Features and Their Relation to Processes and Classification, in: Interpretation of Micromorphological Features of Soils and Regoliths. Elsevier, pp. 15–35. https://doi.org/10.1016/B978-0-444-53156-8.00002-7

1505 Stoops, G., Schaefer, C.E.G.R., 2010. Pedoplasmation, in: Interpretation of Micromorphological
1506 Features of Soils and Regoliths. Elsevier, pp. 69–79. https://doi.org/10.1016/B978-0-444-53156-
1507 8.00005-2

1508 Stuiver, M., Reimer, P.J., 1993. Extended 14C database and revised Calib 3.0 14C Age Calibration
1509 program. Radiocarbon 35, 215–230.

1510 Styring, A., Rösch, M., Stephan, E., Stika, H.-P., Fischer, E., Sillmann, M., Bogaard, A., 2017.
1511 Centralisation and long-term change in farming regimes: Comparing agricultural practices in
1512 Neolithic and Iron Age south-west Germany, in: Proceedings of the Prehistoric Society. pp. 357–
1513 381. https://doi.org/10.1017/ppr.2017.3

1514 Trément, F., Argant, J., Breheret, J.-G., Cabanis, M., Dousteyssier, B., Fourmont, A., Fournier, G.,
1515 Liabeuf, R., Loison, G., Lopez-Saez, J.-A., Macaire, J.-J., Marinval, P., Mennessier-Jouannet, C.,
1516 Milcent, P.-Y., Prat, B., Rialland, Y., Vernet, G., 2007. Un ancien lac au pied de l'oppidum de
1517 Gergovie (Puy-de-Dôme). Gallia 64, 289–351.

1518 Usai, M.R., 2001. Textural Pedofeatures and Pre-Hadrian's Wall Ploughed Paleosols at Stanwix,
1519 Carlisle, Cumbria, U.K. J. Archaeol. Sci. 28, 541–553. https://doi.org/10.1006/jasc.2001.0609

1520 Van der Leeuw, S.E., Audouze, F., Berger, J.F., Durand-Dastès, F., Favory, F., Fiches, J.L., Gazenbeek,
1521 M., Girardot, J.J., Mathian, H., Nuninger, L., Odiot, T., Pumain, D., Raynaud, C., Sanders, L.,
1522 Tourneux, F.P., Verhagen, P., Zannier, M.P., 2005. Climate, hydrology, land use, and
1523 environmental degradation in the lower Rhone Valley during the Roman period. Comptes
1524 Rendus - Geosci. 337, 9–27. https://doi.org/10.1016/j.crte.2004.10.018

1525 van Geel, B., Heijnis, H., Charman, D.J., Thompson, G., Engels, S., 2014. Bog burst in the eastern
1526 Netherlands triggered by the 2.8 kyr BP climate event. Holocene 24, 1465–1477.
1527 https://doi.org/10.1177/0959683614544066

1528 Verstraeten, G., 2015. Quantification of human-environment interactions in the past. Anthropocene
1529 8, 1–5. https://doi.org/10.1016/j.ancene.2015.06.002

1530 Vliet-Lanoë, B. Van, 2010. Frost Action, in: Interpretation of Micromorphological Features of Soils and
1531 Regoliths. Elsevier, pp. 81–108. https://doi.org/10.1016/B978-0-444-53156-8.00006-4

1532 Vrydaghs, L., 2017. Opal Sponge Spicules. Archaeol. Soil Sediment Micromorphol., Wiley Online
1533 Books. https://doi.org/doi:10.1002/9781118941065.ch20

1534 Wang, S., Ge, Q., Wang, F., Wen, X., Huang, J., 2013. Abrupt climate changes of Holocene. Chinese
1535 Geogr. Sci. 23, 1–12. https://doi.org/10.1007/s11769-013-0591-z

1536 Wanner, H., Beer, J., Bütikofer, J., Crowley, T.J., Cubasch, U., Flückiger, J., Goosse, H., Grosjean, M.,
1537 Joos, F., Kaplan, J.O., Küttel, M., Müller, S.A., Prentice, I.C., Solomina, O., Stocker, T.F., Tarasov,
1538 P., Wagner, M., Widmann, M., 2008. Mid- to Late Holocene climate change: an overview. Quat.
1539 Sci. Rev. 27, 1791–1828. https://doi.org/10.1016/j.quascirev.2008.06.013

1540 Wedepohl, K.H., 1978. Handbook of geochemistry. Springer-Verlag.

1541